

Frequency and time domain inspiral templates for comparable mass compact binaries in eccentric orbits

Sashwat Tanay, Maria Haney, and Achamveedu Gopakumar
Tata Institute of Fundamental Research, Mumbai 400005, Maharashtra, India
(Dated: May 17, 2016)

Inspiring compact binaries with non-negligible orbital eccentricities are plausible gravitational wave (GW) sources for the upcoming network of GW observatories. In this paper, we present two prescriptions to compute post-Newtonian (PN) accurate inspiral templates for such binaries. First, we adapt and extend the post-circular scheme of Yunes *et al.* [Phys. Rev. D 80, 084001 (2009)] to obtain a Fourier-domain inspiral approximant that incorporates the effects of PN-accurate orbital eccentricity evolution. This results in a fully analytic frequency-domain inspiral waveform with Newtonian amplitude and 2PN order Fourier phase while incorporating eccentricity effects up to sixth order at each PN order. The importance of incorporating eccentricity evolution contributions to the Fourier phase in a PN consistent manner is also demonstrated. Second, we present an accurate and efficient prescription to incorporate orbital eccentricity into the quasi-circular time-domain `TaylorT4` approximant at 2PN order. New features include the use of rational functions in orbital eccentricity to implement the 1.5PN order tail contributions to the far-zone fluxes. This leads to closed form PN-accurate differential equations for evolving eccentric orbits and the resulting time-domain approximant is accurate and efficient to handle initial orbital eccentricities ≤ 0.9 . Preliminary GW data analysis implications are probed using match estimates.

PACS numbers: 04.30.-w, 04.80.Nn, 97.60.Lf

I. INTRODUCTION

Coalescing comparable mass compact binaries are the expected workhorse GW sources for the upcoming second generation kilometer sized laser interferometer systems [1]. For example, a network of GW observatories, such as Advanced LIGO (aLIGO) [2], Virgo [3], and Kagra [4], may be able to detect roughly 5 – 50 GW events/year, provided the beamed short Gamma-ray bursts (GRBs) are due to the merger of stellar mass compact binaries [5]. The stellar mass compact binaries, containing neutron stars (NSs) and black holes (BHs), are expected to shed their formation eccentricities due to the gravitational radiation reaction [6, 7]. This is why the Hulse-Taylor binary pulsar whose present orbital period and eccentricity are ~ 8 hr and ~ 0.6 , respectively [8], will have an orbital eccentricity $\sim 10^{-6}$ when GW driven inspiral brings its orbital frequency to few Hertz. Therefore, isolated compact binaries are expected to be in quasi-circular orbits when they spiral into the frequency windows of terrestrial GW observatories. This makes coalescing compact binaries in quasi-circular orbits the most promising GW sources for these observatories. Additionally, there exist several quasi-circular inspiral waveform families to extract these weak GW signals from the noisy data streams [9].

Very recently, Huerta *et al.* argued that aLIGO type observatories could detect roughly 0.1 – 10 eccentric inspirals per year up to redshift $z \sim 0.2$ [10]. This study was influenced by a number of recent investigations that explored several plausible astrophysical mechanisms for producing aLIGO relevant compact binaries with non-negligible eccentricities. These observationally unconstrained short period compact binary formation scenarios

include dynamical capture in dense stellar environments, present in both galactic central regions and globular clusters, as well as tidal capturing of compact objects by neutron stars (see for example Refs. [11–13]). Detailed listing of various astrophysical scenarios and mechanisms for producing ultra compact eccentric binaries that will retain residual eccentricities for both ground and space-based GW observatories can be found in Refs. [10, 14, 15]. Therefore, it is possible that the data streams of aLIGO type observatories may contain GWs from eccentric inspirals. This motivated us to construct PN-accurate and computationally efficient waveform families to model inspiral GWs from compact binaries in eccentric orbits.

In the case of non-spinning compact binaries inspiraling along quasi-circular orbits, `TaylorT4` and `TaylorF2` are popular models that provide appropriate interferometric response functions in the time and frequency domain, respectively [9, 16]. These models, usually termed as approximants [17], use PN approximation to general relativity to describe the frequency and phase evolution of GWs from compact binaries [18]. The PN approximation is also employed to specify the amplitudes of the two polarization states, namely h_{\times} and h_{+} . In this context, the PN approximation provides general relativity based corrections to the Newtonian (or quadrupolar) estimates such that n PN corrections give contributions that are accurate up to the relative $(v/c)^{2n}$ order beyond their Newtonian estimate, where v and c are the orbital and light speeds, respectively. To incorporate higher order PN contributions to the frequency evolution as well as to the amplitudes of h_{\times} and h_{+} , these approximants employ the dimensionless post-Newtonian expansion parameter x [19]. This gauge-invariant parameter is defined as $x \equiv (Gm\omega/c^3)^{2/3}$, where m is the total binary mass

while ω stands for the orbital (angular) frequency. Currently, the state of the art 3.5PN order `TaylorT4` approximant provides corrections to the frequency evolution that are accurate to $\mathcal{O}(x^{3.5})$ beyond the quadrupolar (Newtonian) estimate [20]. In contrast, the fully analytic 3.5PN order `TaylorF2` approximant employing 3.5PN-accurate Fourier phase is widely used to model quasi-circular inspiral templates in the frequency domain. At present, the amplitude corrected GW polarization states for compact binaries in circular orbits are available to the relative 3PN order [21]. Unfortunately, quasi-circular inspiral waveforms are substantially suboptimal to detect GWs from compact binaries with residual eccentricity > 0.05 [22]. In light of the above discussions, it should be of definite interest to extend these approximants by including the effects of non-negligible orbital eccentricities.

In the first part of the paper, we incorporate the effects of PN-accurate orbital eccentricity evolution into the Fourier phase of the 2PN-accurate circular `TaylorF2` approximant. This is done by adapting and extending the post-circular (PC) scheme of Yunes *et al.* [14]. In this approach, one first computes eccentricity induced higher ω -based harmonic corrections to both the amplitudes and phases of the two GW polarization states. This leads to the data analysis relevant *response function* $h(t)$ for compact binaries inspiraling along eccentric orbits. The frequency-domain inspiral templates were constructed by invoking the *Stationary Phase Approximation (SPA)*, detailed in Ref. [23], on this $h(t)$. To obtain fully analytic frequency-domain inspiral templates, Ref. [14] also adapted and extended the idea of an asymptotic eccentricity invariant, introduced in Ref. [24]. This allowed Yunes *et al.* to write down an analytic expression for the orbital eccentricity in terms of ω , its initial value ω_0 and e_0 , the value of orbital eccentricity at ω_0 , such that the uncontrolled errors are of $\mathcal{O}(e_0^9)$. With the help of these ingredients, Ref. [14] explicitly computed $\tilde{h}(f)$, the frequency-domain version of $h(t)$, while incorporating only the Newtonian (quadrupolar) order contributions both in the amplitudes and phases of the two GW polarization states. Very recently, Ref. [10] developed an enhanced post-circular (EPC) formalism to extend the PN-accuracy of the Fourier phase of the above $\tilde{h}(f)$. For this purpose, Huerta *et al.* computed certain 3.5PN order eccentric contributions to the Fourier phase of the circular `TaylorF2` approximant. This was done by defining an eccentricity dependent velocity function from the quadrupolar order Fourier phase of Ref. [14]. This modified velocity function was then incorporated into the Fourier phase expression for the 3.5PN-accurate quasi-circular `TaylorF2` approximant. Indeed, it was noted in Ref. [10] that the EPC model does not provide a consistent PN extension of the Newtonian order Fourier phase of the PC scheme. However, its simplicity turned out to be very useful for pursuing preliminary GW data analysis and astrophysical implications associated with detecting eccentric inspirals with aLIGO type observatories. Notably, the 3.5PN order EPC $\tilde{h}(f)$ was employed to show

that aLIGO could observe $\sim 0.1 - 10$ eccentric inspirals per year out to $z \sim 0.2$ [10].

In this paper, we provide an approach to incorporate eccentricity contributions in a PN consistent manner to the quadrupolar order $\tilde{h}(f)$ of Ref. [14]. This is mainly achieved by incorporating the effects of PN-accurate orbital eccentricity evolution into the Fourier phase of the above $\tilde{h}(f)$. A crucial ingredient is the derivation of a 2PN-accurate expression for a certain orbital eccentricity e_t as a bivariate expansion in terms of x and e_0 . The eccentricity parameter e_t , referred to as the time-eccentricity, appears in the Keplerian-type parametric solution to the PN-accurate compact binary dynamics [25, 26]. This parameter is required to characterize the orbital ellipticity while modeling GWs from compact binaries inspiraling along PN-accurate eccentric orbits [27]. With the help of our 2PN-accurate expression for e_t and Ref. [14], we derive the PN-accurate Fourier phase of $\tilde{h}(f)$. The resulting fully analytic frequency-domain approximant provides inspiral waveforms with Newtonian amplitudes and 2PN order Fourier phase while incorporating eccentricity evolution contributions accurate up to sixth order in e_0 at each PN level.

To check the accuracy of our approach, we first explore how our approximate analytic e_t estimates differ from their 2PN-accurate numerical $e_t(\omega)$ counterparts that treat e_t in an exact manner. The maximum differences turned out to be $\leq 2\%$ of their initial values e_0 for a wide variety of binary and orbital parameters even during the late inspiral. We also show the importance of incorporating eccentricity contributions to the Fourier phase in a PN consistent manner. This is essentially achieved by computing three different estimates for the accumulated GW cycles (\mathcal{N}) in the aLIGO frequency window while using the $l = 2$ harmonics of eccentric inspirals. In this paper, the term ‘aLIGO frequency window’ is used to indicate the lower and upper limits for x , namely $x_{\text{low}} = (Gm\pi 10/c^3)^{2/3}$ and $x_{\text{high}} = 1/6$. This indicates that we let the orbital evolution begin from a fiducial GW frequency of 10 Hz and end it at the last stable orbit of the binary, specified by $6Gm/c^2$. Let us stress that for brevity we henceforth use ‘aLIGO frequency window’ as a short hand to denote the limits of binary evolution in the frequency windows of various advanced GW observatories like aLIGO, Virgo and Kagra. The above mentioned \mathcal{N} estimates arise from three different analytic expressions for the orbital phase $\phi(\omega, \omega_0, e_0)$ as well as our eccentric extension of the 2PN-accurate `TaylorT4` approximant, detailed in Sec. III, that treats e_t effects in an exact manner. The analytic expressions for $\phi(\omega, \omega_0, e_0)$ are based on our 2PN-accurate expression for e_t , the EPC approach and the PC approach, supplemented by the 2PN-accurate circular expression for $\phi(\omega)$. We find that the \mathcal{N} estimates, based on our PN-accurate $\phi(\omega, \omega_0, e_0)$, are comparatively closer to those estimates arising from the eccentric extension of the 2PN-accurate `TaylorT4` approximant. This is a desirable feature, as our time-domain eccentric ap-

proximant can be treated as an improved version of the x -model which was calibrated against a numerical relativity simulation in Ref. [28]. In our view, this also points to the importance of including eccentricity contributions in a PN consistent manner while computing Fourier-domain inspiral templates for eccentric inspirals. However, it will be desirable to include explicitly PN effects due to periastron advance, higher order radiation reaction and spins into our analytic $\tilde{h}(f)$. The resulting $\tilde{h}(f)$ should be useful to construct computationally efficient PN-accurate Fourier-domain search templates for compact binaries in inspiraling eccentric orbits.

In the second part of the paper, we describe our prescription to include the effects of orbital eccentricity into the time-domain `TaylorT4` approximant in an accurate and efficient manner. This approximant turned out to be the natural candidate for incorporating eccentricity effects in an efficient and exact manner among various time domain circular approximants like `TaylorT1`, `TaylorT2`, `TaylorT3` and `TaylorT4`. We adapt the phasing formalism, detailed in Ref. [27], while employing the gauge-invariant x parameter as done in Ref. [28]. This approach systematically incorporates the fact that GW signals emitted by compact binaries in inspiraling eccentric orbits contain *three different time scales*, namely the orbital, periastron precession and radiation-reaction time scales. In the present implementation, the orbital dynamics is fully 2PN-accurate. Therefore, this time-domain approximant models GWs from non-spinning compact binaries that move along 2PN-accurate precessing eccentric orbits while inspiraling under the influence of GW emission that is fully 2PN accurate. We provide four PN-accurate differential equations to incorporate secular variations, both conservative and dissipative, into the orbital variables that are present in the PN-accurate expressions for the two GW polarization states. In contrast, the orbital time scale variations are included with the help of the 2PN-accurate Keplerian-type parametric solution in harmonic gauge [26]. The use of a modified Mikkola's method, detailed in Ref. [29], to solve the 2PN-accurate Kepler equation ensures that orbital time scale variations in the dynamical variables are implemented in an accurate and computationally inexpensive way. Another new feature is the use of *rational functions* in orbital eccentricity to incorporate the leading order tail contributions to the dissipative dynamics. This allows us to replace the infinite sum of Bessel functions in terms of which the 1.5PN order tail contributions to the far-zone fluxes are usually specified [30, 31]. The use of rational functions ensures that our approach can

tackle initial eccentricities ≤ 0.9 in a computationally efficient way. We briefly contrast our approach with the the x -model of Ref. [28] and point out that further investigations will be required to estimate the comparative accuracies and efficiencies of the two approaches. With the help of match estimates, we show that our time-domain prescription that treats eccentricity in an exact manner should be required to faithfully capture eccentric inspirals with $e_0 \geq 0.2$.

The paper is organized in the following way. In Sec. II we present our approach to incorporate PN order eccentric contributions to the Fourier phase of $\tilde{h}(f)$ given in Ref. [14] and probe its salient features. The formalism with which we incorporate the effects of orbital eccentricity into the time-domain quasi-circular `TaylorT4` approximant is detailed in Sec. III. We also probe preliminary data analysis implications of our approximant in this section. A brief summary, possible implications and extensions are listed in Sec. IV.

II. ANALYTIC $\tilde{h}(f)$ FOR ECCENTRIC INSPIRALS WITH 2PN ORDER FOURIER PHASE

We begin with a brief review of the PC approach of Ref. [14] to compute an analytic frequency-domain response function with quadrupolar (Newtonian) order amplitude and phase for eccentric inspirals. The extension of this approach to obtain analytical $\tilde{h}(f)$ with 2PN-accurate Fourier phase and its preliminary implications are presented in Sec. II B. In this extension, we focus on the effect of PN-accurate eccentricity (and frequency) evolution on the Fourier phase. However, the influence of periastron advance on the harmonic structure of GW polarizations states, as explored in Ref. [32], and its influence on $\tilde{h}(f)$ is not pursued in the present extension.

A. Newtonian order post-circular $\tilde{h}(f)$

The approach of Ref. [14] begins by expressing h_{\times} and h_{+} for compact binaries in eccentric orbits as a sum over harmonics. These harmonics are defined in terms of the mean anomaly $l = 2\pi F(t - t_0)$, where F is the orbital frequency while t_0 is some initial epoch. The quadrupolar (Newtonian) order expressions for the two polarization states that incorporate eccentricity corrections up to $\mathcal{O}(e_i^8)$, given in Ref. [14], take the form

$$h_{+, \times}(t) = -\frac{Gm\eta}{c^2 D_L} x \sum_{j=1}^{10} \left[C_{+, \times}^{(j)} \cos jl + S_{+, \times}^{(j)} \sin jl \right], \quad (2.1)$$

where η and D_L stand for the symmetric mass ratio and the luminosity distance, respectively. The symmetric

mass ratio η of a binary consisting of individual masses

m_1 and m_2 is defined to be $\eta = (m_1 m_2)/m^2$, where the total mass $m = m_1 + m_2$. The amplitudes $C_{\times,+}^{(j)}$ and $S_{\times,+}^{(j)}$ are power series in e_t whose coefficients are trigonometric functions of the two angles ι, β that specify the line of sight vector in a certain inertial frame. Recall that the time eccentricity parameter e_t is identical to the usual orbital eccentricity at the Newtonian order. The explicit expressions for these amplitudes, accurate up to $\mathcal{O}(e_t^8)$, are provided by Eqs. (B) in Ref. [14]. The above two expressions for $h_{\times,+}$ arise from the Newtonian order GW polarizations, derived in Ref. [33], in terms of the or-

bital eccentricity and trigonometric functions of the true anomaly ϕ, ι and β . The harmonic structure of Eq. (2.1) is obtained with the help of infinite series expansions for $\sin \phi$ and $\cos \phi$ in terms of $\sin jl$ and $\cos jl$. The coefficients of $\sin jl$ and $\cos jl$ involve orbital eccentricity and the Bessel functions of first kind $J_j(j e_t)$. The explicit harmonic content of Eq. (2.1) is the result of Taylor expanding the eccentricity factors and $J_j(j e_t)$ in the small eccentricity limit.

The detector strain or interferometric response function for GWs is defined to be

$$h(t) = F_+(\theta_S, \phi_S, \psi_S) h_+(t) + F_\times(\theta_S, \phi_S, \psi_S) h_\times(t), \quad (2.2)$$

where $F_{\times,+}(\theta_S, \phi_S, \psi_S)$ are the two detector antenna patterns. These quantities depend on the right ascension and declination of the source as well as the polarization angle ψ_S [34]. With the above equations for h_\times and h_+ , it is fairly straightforward to obtain $h(t)$ for GWs from compact binaries in eccentric orbits. The resulting expression for the response function for eccentric inspirals, given by Eq. (4.21) of Ref. [14], reads

$$h(t) = -\frac{Gm\eta}{c^2 D_L} \left(\frac{Gm\omega}{c^3} \right)^{2/3} \sum_{j=1}^{10} \alpha_j \cos(jl + \phi_j), \quad (2.3)$$

where $\alpha_j = \text{sgn}(\Gamma_j) \sqrt{\Gamma_j^2 + \Sigma_j^2}$ and $\phi_j = \arctan\left(-\frac{\Sigma_j}{\Gamma_j}\right)$. The two new functions, Γ_j and Σ_j , are defined as $\Gamma_j = F_+ C_+^{(j)} + F_\times C_\times^{(j)}$ and $\Sigma_j = F_+ S_+^{(j)} + F_\times S_\times^{(j)}$, respectively. Note that the above ϕ_j should not be confused with the true anomaly ϕ . To obtain $h(t)$ for GWs from inspiraling binaries in eccentric orbits, we need to specify how $\omega = 2\pi F$ and e_t vary in time. At the quadrupolar order, the temporal evolution for ω and e_t is defined by

$$\frac{d\omega}{dt} = \frac{(Gm\omega)^{5/3} \omega^2 \eta}{5c^5 (1-e_t^2)^{7/2}} \left\{ 96 + 292 e_t^2 + 37 e_t^4 \right\}, \quad (2.4a)$$

$$\frac{de_t}{dt} = -\frac{(Gm\omega)^{5/3} \omega \eta e_t}{15c^5 (1-e_t^2)^{5/2}} \left\{ 304 + 121 e_t^2 \right\}, \quad (2.4b)$$

adapted from Refs. [6, 35]. Clearly, we need to solve these two coupled differential equations numerically to obtain $\omega(t)$ and $e_t(t)$. This makes the procedure to obtain $h(t)$ for GWs from inspiraling eccentric binaries computationally expensive compared to quasi-circular inspirals.

Fortunately, it is possible to obtain an analytical frequency-domain version of the above $h(t)$ in the small eccentricity limit. To compute such a $\tilde{h}(f)$, one requires the method of SPA to implement the required Fourier Transform. This was essentially demonstrated at the leading order in initial eccentricity in Ref. [24] and extended to $\mathcal{O}(e_0^8)$ in Ref. [14]. The Fourier Transform of $h(t)$, given by Eq. (4.29) in Ref. [14], may be written as

$$\tilde{h}(f) = \tilde{\mathcal{A}} \left(\frac{Gm\pi f}{c^3} \right)^{-7/6} \sum_{j=1}^{10} \xi_j \left(\frac{j}{2} \right)^{2/3} e^{-i(\pi/4 + \Psi_j)}, \quad (2.5)$$

where the amplitude coefficients $\tilde{\mathcal{A}}$ and ξ_j are given by

$$\tilde{\mathcal{A}} = -\left(\frac{5\eta\pi}{384} \right)^{1/2} \frac{G^2 m^2}{c^5 D_L}, \quad (2.6a)$$

$$\xi_j = \frac{(1-e_t^2)^{7/4}}{\left(1 + \frac{73}{24}e_t^2 + \frac{37}{96}e_t^4\right)^{1/2}} \alpha_j e^{-i\phi_j(f/j)}. \quad (2.6b)$$

To operationalize the above expression, a number of steps are required. First, the coefficients ξ_j should be Taylor expanded around $e_t = 0$, leading to certain explicit expressions for ξ_j in terms of $e_t, F_\times, F_+, \iota$ and β . The Eqs. (C1) of Ref. [14] list such expressions for ξ_j that are accurate to $\mathcal{O}(e^8)$ while choosing $\iota = \beta = 0$. In the second step, one specifies with the help of the SPA how e_t and Ψ_j depend on the Fourier frequency f . Following Ref. [14], the expression for $\Psi_j(f)$ is given by

$$\Psi_j[F(t_0)] = 2\pi \int^{F(t_0)} \tau' \left(j - \frac{f}{F'} \right) dF'. \quad (2.7)$$

where τ stands for F/\dot{F} . Additionally, the integrals on the right hand side should be evaluated at the stationary point t_0 which is defined by $F(t_0) = f/j$.

A close inspection reveals that the τ integrals can only be tackled in an approximate manner due to the GW induced evolution of e_t . Therefore, the third step involves obtaining an approximate expression for e_t in terms of ω, ω_0 and e_0 . Subsequently, one evaluates the above τ integrals analytically with the help of such an e_t relation. An approximate frequency evolution for e_t is obtained by first computing the ratio $d\omega/de_t = \omega \kappa_N(e_t)$ using Eqs.(2.4a) and (2.4b) for $\dot{\omega}$ and \dot{e}_t . It turns out that κ_N depends only on e_t at the dominant quadrupolar order. This allows one to write $d\omega/\omega = \kappa'_N(e_t, e_0) de_t$ which can be integrated analytically. The resulting expression may be written as $\omega/\omega_0 = \kappa'(e_t, e_0)$ and the explicit functional form of $\kappa'(e_t, e_0)$, extracted from Eq. (62) of Ref. [27], reads

$$\kappa'(e_t, e_0) = \frac{e_0^{18/19} (304 + 121 e_0^2)^{1305/2299}}{(1 - e_0^2)^{3/2}} \frac{(1 - e_t^2)^{3/2}}{e_t^{18/19} (304 + 121 e_t^2)^{1305/2299}}. \quad (2.8)$$

It is possible to invert the above expression in the limit $e_t \ll 1$ to obtain e_t in terms of e_0, ω and ω_0 . At the

leading order in e_0 , one obtains

$$e_t \sim e_0 \chi^{-19/18} + \mathcal{O}(e_0^3), \quad (2.9)$$

where χ is defined as $\omega/\omega_0 = F/F_0$. The above equation motivated Ref. [24] to introduce an asymptotic eccentricity invariant. It is fairly straightforward to compute τ in terms of ω, ω_0 and e_0 as

$$\tau \sim \frac{5}{96 \eta x^4} \left(\frac{G m}{c^3} \right) \left[1 - \frac{157 e_0^2}{24} \chi^{-19/9} + \mathcal{O}(e_0^4) \right]. \quad (2.10)$$

The above expression for τ allows one to evaluate analytically the following indefinite integral

$$2\pi \int \tau' \left(j - \frac{f}{F'} \right) dF'. \quad (2.11)$$

Clearly, this integral will have to be evaluated at the stationary point t_0 , namely $j \dot{t}_0 = 2\pi f$, to obtain $\Psi_j(\omega(t_0))$ as noted in Ref. [14]. This leads to the following expression for Ψ_j , accurate up to $\mathcal{O}(e_0^2)$,

$$\Psi_j \sim j \phi_c - 2\pi f t_c - \frac{3}{128 \eta} \left(\frac{G m \pi f}{c^3} \right)^{-5/3} \left(\frac{j}{2} \right)^{8/3} \left[1 - \frac{2355 e_0^2}{1462} \chi^{-19/9} + \mathcal{O}(e_0^4) \right], \quad (2.12)$$

where ϕ_c and t_c are the orbital phase at coalescence and the time of coalescence, respectively. The following points are worth mentioning: The χ , appearing in the above equations for e_t and Ψ_j , now stands for f/f_0

due to the use of the stationary phase condition. To ensure that $e_t(f_0) = e_0$, one is required to rescale F_0 such that $F_0 \rightarrow f_0/j$. We have verified that the above expression is indeed consistent with Eq. (4.28) of Ref. [14] that

employs the chirp mass to characterize the binary.

This sub-section may be summarized as follows. The stationary phase approximation can be applied to compute analytically the Fourier transform of the time-domain detector strain $h(t)$ for quadrupolar order GWs from compact binaries in inspiraling eccentric orbits. The resulting frequency-domain response function is symbolically given by Eq. (2.5). To operationalize $\tilde{h}(f)$, one needs to specify the explicit functional dependence of ξ_j , e_t and Ψ_j on f . The expressions for e_t and Ψ_j that are accurate to leading order in e_0 are given by Eqs. (2.9) and (2.12) where $\chi = f/f_0$ due to the use of the stationary-phase condition. Additionally, we need to re-expand ξ_j in the limit $e_t \ll 1$ and employ an appropriate $e_t(f)$ expression to obtain the fully analytic $\tilde{h}(f)$. It is fairly

straightforward to compute higher order corrections in terms of e_0 to e_t up to $\mathcal{O}(e_0^7)$ and to extend Ψ_j to $\mathcal{O}(e_0^8)$ as done in Ref. [14]. In the next section, we improve their results by incorporating into Ψ_j effects of PN-accurate eccentricity.

B. Restricted $\tilde{h}(f)$ with 2PN order Fourier phase

We begin by displaying the time-domain response function for eccentric binary inspirals that incorporates the first eight harmonics with quadrupolar order amplitudes. The aim of this subsection, as noted earlier, is to obtain an analytic frequency-domain version of such a detector strain. Invoking Ref. [14], we write

$$h(t) = -\frac{Gm\eta}{c^2 D_L} x \sum_{j=1}^8 \alpha_j (\cos \phi_j \cos jl - \sin \phi_j \sin jl) . \quad (2.13)$$

A different restriction on the harmonic index j arises as our PN-accurate Fourier phase will be accurate only up to $\mathcal{O}(e_0^6)$ at each PN order. Similar restrictions apply while explicitly implementing the quantities α_j and ϕ_j , given by Eqs. (4.22) of Ref. [14] in the above equation for $h(t)$. A non-rigorous argument for restricting the harmonic index j to six is presented towards the end of Sec. III. The temporally evolving $h(t)$ of Ref. [14], in principle, is obtained by allowing e_t and ω to vary in time due to the quadrupolar (Newtonian) order gravitational wave emission. However, the time evolution of the above $h(t)$ is specified with the help of 2PN-accurate differential equations for ω and e_t , given by our Eqs. (3.12a) and (3.12b) respectively. These 2PN-accurate expressions include certain ‘instantaneous’ contributions to $d\omega/dt$ and de_t/dt , given by Eqs. (6.14),(6.15a),(6.15b) and (C6), Eqs. (6.18),(6.19a), (6.19b) and (C10) of Ref. [36], respectively. The 1.5PN order hereditary contributions to $d\omega/dt$ and de_t/dt are computed with the help of leading order contributions to energy and angular momentum fluxes, given in Eqs. (6.8) and (5.29) of Ref. [36]. The use of above mentioned equations of Ref. [36] in this paper implies that we employ the harmonic gauge to obtain $h(t)$ for eccentric inspirals. The resulting $h(t)$ models detector

strain for GWs from compact binaries inspiraling under the influence of 2PN-accurate GW emission along Newtonian eccentric orbits. In this section, we compute the Fourier transform of the resulting $h(t)$ analytically while keeping terms up to $\mathcal{O}(e_t^6)$ at each PN order. In contrast, the next section provides GW polarization states for compact binaries inspiraling under the influence of 2PN-accurate GW emission along 2PN-accurate eccentric orbits.

We begin by listing our main results and then explain in detail how we derived them. The expression for $\tilde{h}(f)$ with 2PN level Fourier phase and Newtonian order amplitude reads

$$\tilde{h}(f) = \tilde{\mathcal{A}} \left(\frac{Gm\pi f}{c^3} \right)^{-7/6} \sum_{j=1}^8 \xi_j \left(\frac{j}{2} \right)^{2/3} e^{-i(\pi/4 + \Psi_j)} , \quad (2.14)$$

where the quantities ξ_j are polynomials in e_t whose coefficients are complex functions of F_+ , F_\times , t , β and arise from Eq. (2.6b). For the present investigation, the ξ_j coefficients need only be accurate to $\mathcal{O}(e_t^6)$ due to the above j restriction. The main result of this section, namely, the explicit 2PN order expression for Ψ_j that incorporates $\mathcal{O}(e_0^2)$ corrections at each PN order is given by

$$\Psi_j \sim j\phi_c - 2\pi f t_c - \frac{3}{128\eta} \left(\frac{Gm\pi f}{c^3} \right)^{-5/3} \left(\frac{j}{2} \right)^{8/3} \left\{ 1 - \frac{2355e_0^2}{1462} \chi^{-19/9} + x \left[\frac{3715}{756} + \frac{55}{9}\eta + \left(\left(-\frac{2045665}{348096} \right. \right. \right. \right. \\ \left. \left. \left. - \frac{128365}{12432}\eta \right) \chi^{-19/9} + \left(-\frac{2223905}{491232} + \frac{154645}{17544}\eta \right) \chi^{-25/9} \right] e_0^2 \right\} + x^{3/2} \left[-16\pi + \left(\frac{65561\pi}{4080} \chi^{-19/9} \right. \right. \\ \left. \left. + \left(-\frac{2045665}{348096} - \frac{128365}{12432}\eta \right) \chi^{-19/9} + \left(-\frac{2223905}{491232} + \frac{154645}{17544}\eta \right) \chi^{-25/9} \right] e_0^2 \right]$$

$$\begin{aligned}
& -\frac{295945\pi}{35088}\chi^{-28/9})e_0^2] + x^2 \left[\frac{15293365}{508032} + \frac{27145}{504}\eta + \frac{3085}{72}\eta^2 + \left[\left(-\frac{111064865}{14141952} - \frac{165068815}{4124736}\eta \right. \right. \right. \\
& \left. \left. \left. - \frac{10688155}{294624}\eta^2 \right) \chi^{-19/9} + \left(-\frac{5795368945}{350880768} + \frac{4917245}{1566432}\eta + \frac{25287905}{447552}\eta^2 \right) \chi^{-25/9} + \left(\frac{936702035}{1485485568} + \frac{3062285}{260064}\eta \right. \right. \right. \\
& \left. \left. \left. - \frac{14251675}{631584}\eta^2 \right) \chi^{-31/9} \right] e_0^2 \right] , \tag{2.15}
\end{aligned}$$

where the use of the stationary phase condition implies that $\chi = f/f_0$ and $x \equiv (Gm\omega(t_0)/c^3)^{2/3}$. This ensures that $x = [(Gm/c^3) \times (2\pi f/j)]^{2/3}$. We have verified that the above expression is consistent with e_0^2 terms

of Eq. (3) in Ref. [37]. Additionally, the following 2PN-accurate analytic expression for e_t is required to specify the frequency dependence of the harmonic coefficients, namely ξ_j :

$$\begin{aligned}
e_t \sim e_0 \left\{ \chi^{-19/18} + x \left(\frac{2833}{2016} - \frac{197}{72}\eta \right) \left[-\chi^{-19/18} + \chi^{-31/18} \right] + x^{3/2} \left(\frac{377\pi}{144} \right) \left[-\chi^{-19/18} + \chi^{-37/18} \right] \right. \\
+ x^2 \left[\left(\frac{77006005}{24385536} - \frac{1143767}{145152}\eta + \frac{43807}{10368}\eta^2 \right) \chi^{-19/18} + \left(-\frac{8025889}{4064256} + \frac{558101}{72576}\eta - \frac{38809}{5184}\eta^2 \right) \chi^{-31/18} \right. \\
\left. \left. + \left(-\frac{28850671}{24385536} + \frac{27565}{145152}\eta + \frac{33811}{10368}\eta^2 \right) \chi^{-43/18} \right] \right\} . \tag{2.16}
\end{aligned}$$

Clearly, the above two expressions incorporate only the leading order initial eccentricity contributions at each PN order and contain uncontrolled terms of $\mathcal{O}(e_0^4)$ and $\mathcal{O}(e_0^3)$, respectively. For this paper, we have extended the above results to obtain 2PN order expressions for Ψ_j and e_t while incorporating initial eccentricity contributions up to $\mathcal{O}(e_0^6)$ and $\mathcal{O}(e_0^5)$, respectively, at each PN order. These lengthy expressions are listed as Eqs. (A3) and (A5) in the Appendix A. This extension of Ref. [14] provides a certain *restricted* PN-accurate Fourier-domain response function for GWs from compact binaries in inspiraling eccentric orbits. Our waveforms are *restricted* as the amplitude contributions to $\tilde{h}(f)$ are at Newtonian order while the Fourier phase contributions are 2PN-accurate. This is the eccentric equivalent to the restricted PN waveform families that incorporate amplitude contributions at the quadrupolar order and employ PN-accurate orbital phase evolution while modeling GWs from quasi-circular inspirals [17]. Such waveform families are influenced by the fact that the technique of *matched filtering* demands PN-accurate modeling of GW phase evolution while constructing inspiral search templates.

In the following, we explain with intermediate steps our approach to compute the 1PN extension of the New-

tonian order Fourier phase, available in Refs. [14, 24]. This demands the extension of the Newtonian relation, namely $e_t = e_0 \chi^{-19/18}$, to incorporate PN and higher order e_0 contributions at every PN order. We observe that these computations are hierarchical at each PN order. This is because the 1PN-accurate $e_t(\chi, e_0)$ relation that incorporates $\mathcal{O}(e_0)$ contributions will be explicitly required while extending it to include $\mathcal{O}(e_0^3)$ terms at the same PN order. In what follows, we detail our approach to compute the 1PN extension of the Newtonian $e_t = e_0 \chi^{-19/18}$ relation. Our prescription demands the computation of 1PN order expression for $d\omega/de_t$ with the help of Eqs. (3.12a) and (3.12b) for $\dot{\omega}$ and \dot{e}_t . This leads to an equation for $d\omega/\omega = \kappa_1(e_t, \omega) de_t$ where

$$\kappa_1 = -\frac{18}{19e_t} - \frac{3}{10108e_t} (-2833 + 5516\eta) \left(\frac{Gm\omega}{c^3} \right)^{2/3} . \tag{2.17}$$

It is important to note that ω terms appear only at the 1PN order. Therefore, we employ the Newtonian accurate $\omega = \omega_0 (e_0/e_t)^{18/19}$, available in Ref. [27], to replace ω in κ_1 . This results in

$$d\omega/\omega \sim \left\{ -\frac{18}{19e_t} - \frac{3}{10108} \left(\frac{e_0^{12/19}}{e_t^{31/19}} \right) (-2833 + 5516\eta) x_0 \right\} de_t , \tag{2.18}$$

where $x_0 = (G m \omega_0 / c^3)^{2/3}$. It is straightforward to integrate the above equation to obtain $\ln \omega - \ln \omega_0$ in terms of e_t, e_0 and ω_0 . We take the exponential of the resulting

expression and perform a bivariate expansion in terms of x_0 and e_t , leading to

$$\omega \sim \left\{ \left(\frac{e_0}{e_t} \right)^{18/19} + x_0 \left(\frac{2833 - 5516}{2128} \eta \right) \left[\left(\frac{e_0}{e_t} \right)^{18/19} - \left(\frac{e_0}{e_t} \right)^{30/19} \right] \right\} \omega_0. \quad (2.19)$$

To extract the 1PN-accurate e_t expression from the above equation, we replace the e_t terms that appear at the x_0 level by the leading order $e_t = e_0 \chi^{-19/18}$. It is possible to invert the resulting expression and obtain e_t as a bi-

variate expansion in terms of e_0 and x_0 . As expected, the expansion requires that $e_0 \ll 1$ and $x_0 \ll 1$, and we obtain the following e_t expression:

$$e_t \sim e_0 \left\{ \chi^{-19/18} + x_0 \left(\frac{2833}{2016} - \frac{197}{72} \eta \right) \left(-\chi^{-7/18} + \chi^{-19/18} \right) \right\}. \quad (2.20)$$

We compute e_t as a bivariate expansion in terms of the PN parameter x and e_0 by noting that $x/x_0 = \chi^{2/3}$. This leads to

$$e_t \sim e_0 \left\{ \chi^{-19/18} + x \left(\frac{2833}{2016} - \frac{197}{72} \eta \right) \left(-\chi^{-19/18} + \chi^{-31/18} \right) \right\}. \quad (2.21)$$

The hierarchical nature of these computations implies that the above expression is explicitly required during the 1PN e_t computation for incorporating $\mathcal{O}(e_0^3)$ terms appearing at the Newtonian and 1PN orders. In this paper, we pursue (and repeat) the above detailed steps to obtain the crucial 2PN-accurate e_t as a bivariate expansion in x and e_0 . This lengthy expression, incorporating $\mathcal{O}(e_0^5)$ corrections at each PN order, is listed as Eq. (A5).

Let us now turn our attention to the computation of the 1PN-accurate Fourier phase. We adapt Ref. [14] and write PN-accurate Ψ_j as

$$\Psi_j[F(t_0)] = 2\pi \int^{F(t_0)} \tau' \left(j - \frac{f}{F'} \right) dF', \quad (2.22)$$

where the PN approximation enters via τ . With the help of Eq. (2.21) for 1PN-accurate $e_t(\omega)$ and Eq. (3.12a) for \dot{x} , it is straightforward to compute 1PN-accurate $\tau \equiv \omega/\dot{\omega}$ as

$$\tau \sim \frac{5}{96 \eta x^4} \left(\frac{G m}{c^3} \right) \left\{ 1 - \frac{157 e_0^2}{24} \chi^{-19/9} + x \left[\frac{743}{336} + \frac{11}{4} \eta + \left(\left[-\frac{444781}{24192} + \frac{30929}{864} \eta \right] \chi^{-25/9} + \left[-\frac{409133}{24192} - \frac{25673}{864} \eta \right] \chi^{-19/9} \right) e_0^2 \right] \right\}. \quad (2.23)$$

The fact that we employ Eq. (2.21) for e_t while computing τ implies that we can only retain $\mathcal{O}(e_0^2)$ contributions both at the Newtonian and 1PN orders. It is now straightforward to integrate analytically the indefinite integral for Ψ_j . The resulting integral is evaluated

at the stationary point t_0 to obtain $\Psi_j(t_0)$. This stationary point t_0 is again defined to be $j \times \dot{l}(t_0) = 2\pi f$, even while invoking PN-accurate τ expression. This leads to the 1PN-accurate Ψ_j expression that includes $\mathcal{O}(e_0^2)$ contributions both at the Newtonian and 1PN orders, namely

$$\begin{aligned} \Psi_j \sim j\phi_c - 2\pi ft_c - \left(\frac{3j}{256\eta}\right) x^{-5/2} \left\{ 1 - \frac{2355e_0^2}{1462}\chi^{-19/9} + x \left[\frac{3715}{756} + \frac{55}{9}\eta + \left(\left[-\frac{2045665}{348096} - \frac{128365}{12432}\eta \right] \chi^{-19/9} \right. \right. \right. \\ \left. \left. \left. + \left[-\frac{2223905}{491232} + \frac{154645}{17544}\eta \right] \chi^{-25/9} \right) e_0^2 \right\}, \end{aligned} \quad (2.24)$$

where the quantities x and χ will have to be evaluated at the stationary point. It is straightforward, though algebraically involved, to extend the above arguments to 2PN order while also keeping higher order e_0 contributions. In Eq. (A3) of appendix A, we list the 2PN order Ψ_j that includes all the $\mathcal{O}(e_0^6)$ contributions at every PN order. In the remainder of this subsection, we probe preliminary implications of our approach.

An obvious aspect of probing our approach should be the accuracy of our bivariate expansion for the orbital eccentricity e_t in terms of x and e_0 , given by Eq. (A5). We first obtain *numerical* estimates e_t^{num} for the orbital eccentricity at certain values of orbital frequency ω by numerically integrating the PN-accurate expressions for $\dot{\omega}$ and \dot{e}_t , given by Eqs. (3.12a) and (3.12b). These numerical estimates are then compared with their *analytic* counterparts, e_t^{ana} , that arise from our Eq. (A5). In Fig. 1, we plot the difference $\Delta e \equiv (e_t^{\text{num}} - e_t^{\text{ana}})$ as a function of x for two different values of initial eccentricity, $e_0 = 0.1$ and 0.4 . Each of the three characteristic bina-

ries in the aLIGO frequency window is considered, i.e., BH-BH, NS-NS and BH-NS configurations with component masses $m_{\text{BH}} = 10M_\odot$ and $m_{\text{NS}} = 1.4M_\odot$, respectively. Our plots reveal that the difference between the *exact* numerical and our approximate analytical estimate for e_t is generally $\leq 2\%$ of the initial value e_0 , even during the late stage of inspiral. This gives us confidence in employing our analytic $e_t(\omega)$ expression while computing the Fourier-domain response function for eccentric inspirals.

We perform another check of our approach by computing 2PN-accurate analytic expression for the orbital phase, $\phi = \int \omega dt \equiv \int (\omega/\dot{\omega}(\omega, e_t)) d\omega$, as a bivariate expansion in x and e_0 . An analytic expression for ϕ is possible as the integrand $\omega/\dot{\omega}$ becomes purely a function of ω when we employ our PN-accurate expression for $e_t(\omega)$ in the evolution equation for $\dot{\omega}$, as given by Eq. (3.12a). This leads to an analytic 2PN order expression for $\phi - \phi_0$, accurate to $\mathcal{O}(e_0^6)$, where ϕ_0 is the initial value $\phi(x_0)$. In what follows, we display our 2PN-accurate $\phi(x)$ that incorporates only the leading order e_0 contributions:

$$\begin{aligned} \phi(x, e_0, F_0) \sim -\frac{x^{-5/2}}{32\eta} \left\{ 1 - \frac{785}{272}e_0^2\chi^{-19/9} + x \left[\frac{3715}{1008} + \frac{55}{12}\eta + \left\{ \left(-\frac{2045665}{225792} - \frac{128365}{8064}\eta \right) \chi^{-19/9} \right. \right. \right. \\ \left. \left. \left. + \left(-\frac{2223905}{274176} + \frac{154645}{9792}\eta \right) \chi^{-25/9} \right\} e_0^2 \right] + x^{3/2} \left[-10\pi + \left(\frac{65561\pi}{2880}\chi^{-19/9} - \frac{295945\pi}{19584}\chi^{-28/9} \right) e_0^2 \right] \right. \\ \left. + x^2 \left[\frac{15293365}{1016064} + \frac{27145}{1008}\eta + \frac{3085}{144}\eta^2 + \left\{ \left(-\frac{111064865}{10948608} - \frac{165068815}{3193344}\eta - \frac{10688155}{228096}\eta^2 \right) \chi^{-19/9} \right. \right. \right. \\ \left. \left. \left. + \left(-\frac{5795368945}{227598336} + \frac{4917245}{1016064}\eta + \frac{25287905}{290304}\eta^2 \right) \chi^{-25/9} + \left(\frac{936702035}{829108224} + \frac{3062285}{145152}\eta - \frac{14251675}{352512}\eta^2 \right) \right. \right. \right. \\ \left. \left. \left. \chi^{-31/9} \right\} e_0^2 \right] \right\}. \end{aligned} \quad (2.25)$$

The 2PN-accurate expression for ϕ that incorporates eccentricity contributions accurate up to $\mathcal{O}(e_0^6)$ is listed in as Eq. (A7) in the appendix.

With this input, we pursue a check on our PN-accurate Ψ_j by computing the accumulated number of GW cycles associated with the $j = 2$ harmonic in the frequency window, specified by $x_{\text{low}} = (Gm\pi 10/c^3)^{2/3}$ and $x_{\text{high}} = 1/6$. We compute and compare four different estimates for $\mathcal{N} = (\phi_{\text{max}} - \phi_{\text{min}})/\pi$, where ϕ_{max} and ϕ_{min} are the values of the orbital phase at the ini-

tial and final values of the x parameter. These four \mathcal{N} estimates are evaluated for each of the classical aLIGO binaries while choosing a number of e_0 values. The first estimate for \mathcal{N} arises from our eccentric extension of the circular **TaylorT4** approximant at 2PN order, denoted by ‘eT4’ and detailed in the next section. This estimate may be treated to be *exact* in e_t since we do not perform any small eccentricity expansion in our time domain approximant. We developed this approximant with the aim to improve certain computational aspects of the x -model

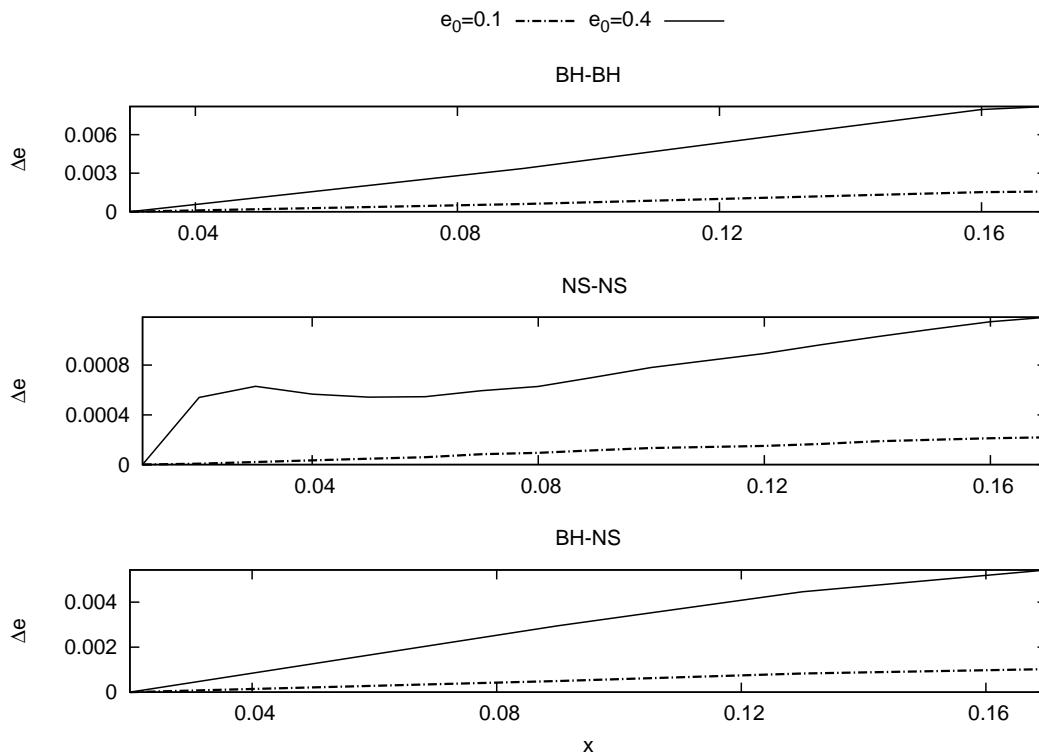


FIG. 1. Plots of Δe as a function of x for three characteristic aLIGO compact binaries, namely BH-BH, NS-NS and BH-NS binaries (in order), having two different initial eccentricities ($e_0 = 0.1, 0.4$). The quantity Δe stands for the difference between the numerical and analytical estimates for e_t , as discussed in the text. The plots show that Δe is usually $\leq 2\%$ of the initial e_0 value, even during the late inspiral ($x \sim 0.16$).

which has been validated against a particular numerical relativity waveform for the eccentric inspiral of an equal-mass binary [28]. The second estimate for \mathcal{N} is obtained by employing our 2PN order (and $\mathcal{O}(e_0^6)$ accurate) expression for ϕ , namely Eq. (A7). In Table I, we list these two estimates for \mathcal{N} in the first two rows while considering the usual BH-BH, NS-NS and BH-NS binaries with initial eccentricities $e_0 = 0, 10^{-3}, 10^{-2}, 0.1, 0.3, 0.4$ and 0.5 . For each (m_1, m_2, e_0) configuration, the fractional difference between the *numerical* and our *analytic* estimate, namely $(\mathcal{N}_{\text{num}} - \mathcal{N}_{\text{ana}}) / \mathcal{N}_{\text{num}} \times 100\%$, is displayed in the parentheses.

A comparison of the evaluated numbers reveals that our 2PN-accurate analytic prescription for ϕ slightly overestimates the accumulated number of GW cycles compared to the numerical estimate for the same (m_1, m_2, e_0) configuration. However, our analytic \mathcal{N} estimates are fairly close to their numerical counterparts even for binaries having moderate initial eccentricity $e_0 \sim 0.4$. Note that binaries with tiny initial orbital eccentricities exhibit higher fractional differences between the numerical and analytic estimates. This can be attributed to the fact that various time-domain PN-accurate quasi-circular inspiral template families indeed provide slightly different \mathcal{N} estimates [9, 16]. We observe sign reversals for the quantity in parentheses at $e_0 \sim 0.5$ when consid-

ering our eccentric time and frequency-domain approximants. This may be treated as a pointer to the range of applicability of our frequency-domain templates.

Additionally, we computed two other \mathcal{N} estimates that are based on two different approaches to obtain an *analytic* expression for ϕ . These numbers are also displayed in Table I along with their fractional differences with respect to their numerical counterparts. The PC + 2PN circular estimate for \mathcal{N} is based on the Newtonian order ‘post-circular’ ϕ of Ref. [14], supplemented by the 1PN, 1.5PN and 2PN circular contributions to ϕ available in Ref. [19]. In contrast, the 2PN order EPC estimate for \mathcal{N} is based on Ref. [10]. This estimate employs a certain 2PN order analytic ϕ that includes eccentricity corrections accurate up to $\mathcal{O}(e_0^6)$. Here, the PN order eccentricity contributions to the phase are computed from the standard 2PN-accurate circular version of ϕ by employing a certain modified velocity function v_{ecc} , given by Eq. (13) of Ref. [10]. It should be noted that the resulting $\phi(x, e_0)$ is not a consistent PN expansion to 2PN order of the PC approach (this aspect of the EPC approach was noted in Ref. [10]). The numbers listed in Table I reveal that the \mathcal{N} estimates obtained with the EPC approach differ substantially from the purely numerical estimates even for binaries with initial eccentricity $e_0 \sim 0.1$. This is troubling since our \mathcal{N}_{num} estimates, as noted above,

e_0	0	0.001	0.01	0.1	0.3	0.4	0.5
$m_1 = 10M_\odot; m_2 = 10M_\odot$							
eT4	607.72	607.76	608.89	590.16	453.58	353.79	249.27
2PN analytic	613.88 (-1.01%)	613.88 (-1.00%)	613.69 (-0.78%)	594.75 (-0.77%)	456.38 (-0.61%)	354.79 (-0.28%)	247.03 (0.89%)
PC + 2PN circular	613.88 (-1.01%)	613.88 (-1.00%)	613.71 (-0.79%)	596.59 (-1.08%)	470.65 (-3.76%)	377.04 (-6.57%)	276.33 (-10.85%)
2PN EPC	613.88 (-1.01%)	613.88 (-1.00%)	613.78 (-0.80%)	603.85 (-2.31%)	521.77 (-15.03%)	449.74 (-27.12%)	361.90 (-45.18%)
$m_1 = 1.4M_\odot; m_2 = 1.4M_\odot$							
eT4	16262.75	16262.70	16257.98	15790.74	12358.47	9818.22	7114.64
2PN analytic	16274.97 (-0.07%)	16274.92 (-0.07%)	16270.20 (-0.07%)	15802.74 (-0.07%)	12368.10 (-0.07%)	9821.08 (-0.02%)	7088.08 (0.37%)
PC + 2PN circular	16274.97 (-0.07%)	16274.92 (-0.07%)	16270.34 (-0.07%)	15816.86 (-0.16%)	12480.40 (-0.98%)	10000.20 (-1.85%)	7332.09 (-3.05%)
2PN EPC	16274.97 (-0.07%)	16274.94 (-0.07%)	16272.36 (-0.08%)	16012.69 (-1.40%)	13866.57 (-12.20%)	11983.00 (-22.04%)	9685.34 (-36.13%)
$m_1 = 10M_\odot; m_2 = 1.4M_\odot$							
eT4	3605.67	3606.06	3607.44	3499.05	2706.34	2124.47	1511.46
2PN analytic	3618.89 (-0.36%)	3618.88 (-0.35%)	3617.78 (-0.28%)	3508.86 (-0.28%)	2711.70 (-0.19%)	2124.69 (-0.01%)	1499.74 (0.77%)
PC + 2PN circular	3618.90 (-0.36%)	3618.89 (-0.35%)	3617.86 (-0.28%)	3516.49 (-0.49%)	2770.61 (-2.37%)	2216.16 (-4.31%)	1619.70 (-7.16%)
2PN EPC	3618.90 (-0.36%)	3618.89 (-0.35%)	3618.31 (-0.30%)	3560.04 (-1.74%)	3078.48 (-13.75%)	2655.95 (-25.01%)	2140.77 (-41.63%)

TABLE I. Four different estimates for the accumulated number of GW cycles associated with the $l = 2$ harmonic of eccentric compact binary inspirals in a frequency window, defined by the earlier specified x_{low} and x_{high} values. The four 2PN order \mathcal{N} estimates are based on one purely numerical (eT4) and three different analytic expressions for ϕ , as detailed in the text. The displayed fractional differences in \mathcal{N} probe how the three analytic \mathcal{N} estimates differ from their purely numerical counterpart. These fractional differences, displayed in the parentheses, are computed by evaluating $([\mathcal{N}_{\text{num}} - \mathcal{N}_{\text{ana}}]/\mathcal{N}_{\text{num}}) \times 100\%$.

are based on an improved version of the numerical relativity calibrated x -model for eccentric inspirals, which treats eccentricity contributions in an exact manner. In comparison, the numbers arising from a modified PC approach which incorporates only circular contributions to ϕ at PN orders are closer to our ‘eT4’ based \mathcal{N} estimates even for $e_0 \sim 0.1$. Observe that all analytic ϕ based \mathcal{N} estimates are close to each other for tiny residual eccentricities like $e_0 = 10^{-3}$ or 10^{-2} . However, we glean from additional evaluations that our 2PN-accurate analytic \mathcal{N} estimates are comparatively closer to their ‘eT4’ counterparts even for compact binaries with non-negligible initial eccentricities like $e_0 = 0.3$. This observation and the various estimates of Table I indicate, in our opinion, the need to incorporate eccentricity evolution contributions in a PN-accurate and consistent manner while computing ϕ and the associated \mathcal{N} estimates.

Note that the integral that defines the orbital phase ϕ is key to obtain the Fourier phase Ψ_j in the SPA, as evident from Eqs. (4.7) and (4.8) in Ref. [14]. This suggests that one should also incorporate eccentricity evolution in a PN-accurate manner while computing the PN-accurate Fourier phase. Therefore, our computation should be

useful to construct accurate and computationally efficient Fourier-domain search templates for compact binaries in inspiraling eccentric orbits. Clearly, further extension and investigation will be required to substantiate this statement.

Let us again summarize our main result. The fully analytic frequency-domain response function, applicable for GW data analysis investigations, with Newtonian order amplitude and 2PN order Fourier phase Ψ_j is given by Eq. (2.14), where the quantities \mathcal{A} and ξ_j are given by Eqs. (2.6a) and (2.6b). Clearly, we need to perform an expansion around small eccentricity e_t while explicitly using the quantities ξ_j . The associated e_t and Ψ_j expressions are given analytically by Eqs. (A5) and (A3). In the next section, we explain the approach that allowed us to provide exact numerical estimates for the accumulated number of GW cycles.

III. INCORPORATING ORBITAL ECCENTRICITY INTO THE TAYLORT4 APPROXIMANT

In this section, we present an accurate and efficient prescription to incorporate orbital eccentricity into the quasi-circular time-domain 2PN-accurate `TaylorT4` approximant. The reasons for focusing only on the `TaylorT4` approximant are the following. We observe that the circular `TaylorT1` approximant provides a differential equation for x which is essentially a ratio of polynomials in x [9]. Therefore, its straightforward eccentric extension requires us to expand the differential equations for x and e_t , given by Eqs. 3.12, as bivariate expansions in terms of x and e_t . The resulting expressions can be used to obtain differential equations for x and e_t as ratios of polynomials in x and e_t . Clearly, this is inconsistent with our efforts to include e_t in an exact manner. Technically, it is also possible to express the differential equations for x and e_t as ratios of polynomials in x while keeping e_t contributions rather exact in e_t . We have worked out such a model to 1PN order, and the resulting approximant turned out to be noticeably slower (computationally) than its eccentric `TaylorT4` counterpart. In our opinion, this version is computationally slower mainly due to the presence of $1/e_t$ terms in the differential equations for e_t . Such terms are rather unavoidable due to the Newtonian-accurate $e_t^2 = 1 + 2EJ^2$ expression, where E and J stand for the reduced orbital energy and angular momentum, respectively. The above two observations prompted us not to pursue `TaylorT1` approximant while including the effects of orbital e_t . We note that the eccentric versions of both `TaylorT2` and `TaylorT3` approximants will also force us to treat e_t in an approximate manner. This restriction is required to obtain analytic expressions for $[\phi(\omega), e_t(\omega), t(\omega)]$ and $[\phi(t), \omega(t), e_t(t)]$ that are crucial to obtain eccentric versions of the circular `TaylorT2` and `TaylorT3` approximants, respectively. Therefore, straightforward eccentric versions of both `TaylorT2` and `TaylorT3` approximants are also in conflict with our desire to treat e_t in an exact manner. In what follows, we briefly sketch how we adapt the GW phasing formalism of Ref. [27] to include e_t effects in an accurate and exact manner into the circular `TaylorT4` approximant. The salient features of our approach and preliminary data analysis implications via certain match estimates are also presented.

A. GW phasing for compact binaries in inspiraling 2PN-accurate eccentric orbits

We begin by listing the dominant quadrupolar contributions to the two independent GW polarization states, $h_+|_Q(t)$ and $h_\times|_Q(t)$, associated with a (m, η) compact binary at a luminosity distance D_L from the observer:

$$h_+(r, \phi, \dot{r}, \dot{\phi})|_Q = -\frac{Gm\eta}{c^4 D_L} \left\{ (1 + C^2) \left[\left(\frac{Gm}{r} + r^2 \dot{\phi}^2 - \dot{r}^2 \right) \cos 2\phi + 2\dot{r}r\dot{\phi} \sin 2\phi \right] + S^2 \left[\frac{Gm}{r} - r^2 \dot{\phi}^2 - \dot{r}^2 \right] \right\}, \quad (3.1a)$$

$$h_\times(r, \phi, \dot{r}, \dot{\phi})|_Q = -\frac{2Gm\eta C}{c^4 D_L} \left[\left(\frac{Gm}{r} + r^2 \dot{\phi}^2 - \dot{r}^2 \right) \sin 2\phi - 2\dot{r}r\dot{\phi} \cos 2\phi \right], \quad (3.1b)$$

where C and S denote $\cos i$ and $\sin i$, respectively, with i being the inclination of the orbital plane with respect to the plane of the sky (see, e.g., Refs. [27, 38]). The dynamical variables r , \dot{r} , ϕ and $\dot{\phi}$ define the polar coordinates of the relative orbital separation vector and their time derivatives.

The GW phasing formalism, developed in Ref. [27], provides an efficient way of implementing both the conservative and reactive contributions to the temporal evolution for these dynamical variables $\{r, \dot{r}, \phi, \dot{\phi}\}$ appearing in Eqs. (3.1). The approach involves splitting the binary dynamics into conservative and dissipative parts, with the latter first entering the compact binary dynamics at the 2.5PN (absolute) order. The 2PN-accurate conservative part of the orbital dynamics is integrable and admits an analytic solution, namely a Keplerian-type parametric solution as detailed in Ref. [26]. The existence of such a 2PN-accurate Keplerian-type parametric solution allows us to express the radial and angular parts of the orbital dynamics as

$$r(t) = r(u(l), \mathcal{E}, \mathcal{J}), \quad \dot{r}(t) = \dot{r}(u(l), \mathcal{E}, \mathcal{J}), \quad (3.2)$$

$$\phi(t) = \lambda + W(u(l), \mathcal{E}, \mathcal{J}), \quad \dot{\phi}(t) = \dot{\phi}(u(l), \mathcal{E}, \mathcal{J}), \quad (3.3)$$

where u and l are the eccentric and mean anomalies of the Keplerian parametrization, while \mathcal{E} and \mathcal{J} stand for the orbital energy and the angular momentum, respectively. The split of the angular variable ϕ explicitly incorporates the effect of periastron advance. This is particularly useful while constructing the frequency spectrum associated with $h_{+, \times}|_Q(t)$ of binaries in inspiraling eccentric orbits (see Ref. [39] for details). The angular variable W is 2π -periodic in u and analytically models orbital time scale variations in ϕ . The remaining two angular-type variables l and λ are defined to be

$$l \equiv n(t - t_0) + c_l, \quad \lambda \equiv (1 + k)n(t - t_0) + c_\lambda, \quad (3.4)$$

where the constants t_0 , c_l and c_λ refer to an initial instant and the respective l and λ values at $t = t_0$. The parameter n is usually referred to as the mean motion while k measures the periastron advance in the time interval $P = 2\pi/n$. It should be noted that the PN-accurate expressions for n and k in terms of \mathcal{E} and \mathcal{J} are gauge-invariant quantities [26, 40].

An additional equation is required to specify how u varies with l and therefore to model explicitly the temporal evolution of our dynamical variables $\{r, \dot{r}, \phi, \dot{\phi}\}$. This is done by solving the following 2PN-accurate Kepler equation (KE) to find $u(l)$. At 2PN order, the KE can be symbolically expressed as

$$l = u - e_t \sin u + l_2(u, \mathcal{E}, \mathcal{J}), \quad (3.5)$$

where l_2 denotes the 2PN corrections to the usual Newtonian KE, namely $l = u - e_t \sin u$. In above equation, e_t stands for a certain ‘time-eccentricity’ parameter of the Keplerian-type parametric solution to the PN-accurate orbital dynamics. A few comments are in order before we explain the details of the GW phasing formalism. It is customary to employ $\omega = n(1+k)$ and e_t to characterize PN-accurate eccentric orbits instead of \mathcal{E} and \mathcal{J} . This ensures that ϕ becomes the required $\omega(t-t_0)$ in the circular limit [36]. Additionally, Ref. [28] showed that inspiral waveforms that employ ω and e_t are in better agreement with their numerical relativity counterparts while considering equal mass eccentric inspirals. These considerations influenced us to employ x and e_t to characterize PN-accurate eccentric orbits as done in Ref. [28, 36, 41]. This implies that our compact binary, evolving under the influence of 2PN-accurate binary dynamics, is fully specified by four initial parameters, namely the values of x, e_t, c_l and c_λ at the initial epoch.

The effects of the dominant (quadrupolar) order GW emission enters the binary dynamics at 2.5PN order. An improved ‘method of variation of constants’ was developed in Ref. [27] to include the effects of GW emission on the conservative 2PN-accurate dynamics of compact binaries in precessing eccentric orbits. This is implemented by demanding that the fully 2.5PN-accurate binary dynamics preserves the same functional form for the dynamical variables $\{r, \dot{r}, \phi, \dot{\phi}\}$. However, the constants of the conservative dynamics are allowed to vary in time. The equations governing the temporal evolutions of these ‘constants’ are given by Eqs. (35) in Ref. [27] and depend, as expected, on the reactive contributions to the binary dynamics. Therefore, this approach allowed Ref. [27] to describe the orbital evolution of eccentric binaries under the influence of fully 2.5PN-accurate orbital motion in a semi-analytic manner.

It was demonstrated in Ref. [27] that the temporal variations of the four constants of integration can be decomposed as a combination of a slow drift and fast oscillations. We may write such variations symbolically as

$$c_\alpha(l) = \bar{c}_\alpha(l) + \tilde{c}_\alpha(l), \quad (3.6)$$

where the subscript α stands for one of the four ‘constants of motion’. (In Ref. [27], these constants were chosen to be $\mathcal{E}, \mathcal{J}, c_l$ and c_λ .) In the above equation, $\bar{c}_\alpha(l)$ denotes the slow (secular) drift, which accumulates over the radiation reaction time scale to induce large changes in $c_\alpha(l)$. The fast (periodic) oscillations denoted by $\tilde{c}_\alpha(l)$ are orbital time scale variations in $c_\alpha(l)$. It turned out that

the effects of such rapidly oscillating contributions are of substantially smaller magnitudes than those associated with the slow drift even while including higher order radiation reaction effects [15, 27]. Therefore, in the present work we consider only the secular time scale variations $\bar{c}_\alpha(t)$ in the orbital dynamics.

Detailed computations reveal that $d\bar{c}_l/dt = d\bar{c}_\lambda/dt \equiv 0$ even while including higher order radiation reaction terms in the orbital dynamics [15, 27]. Additionally, the differential equations for the other two secular variables are identical to the PN-accurate expressions for far-zone energy and angular momentum fluxes, provided \mathcal{E} and \mathcal{J} were used to characterize the orbit. This is a highly desirable result as the far-zone energy and angular momentum fluxes are available to higher PN orders, compared to the 1PN-accurate expressions for the reactive contributions to the orbital dynamics. This allowed Ref. [27] to model orbital dynamics of compact binaries inspiraling under the influence of GW emission at the 2PN order while moving along 2PN-accurate eccentric orbits. It should be noted that this approach does not require one to use \mathcal{E} and \mathcal{J} to specify the orbit. It is indeed possible to use, for example, ω (or x) and e_t to specify our PN-accurate eccentric orbit along with c_l and c_λ . The relevant differential equations for $\bar{\omega}$ and \bar{e}_t are computed with the help of the ‘balance’ arguments. This involves invoking the 2PN-accurate expressions for ω and e_t in terms of \mathcal{E} and \mathcal{J} and employing the balance arguments that equate the time derivatives of \mathcal{E} and \mathcal{J} to the 2PN-accurate far-zone energy and angular momentum fluxes. As a result, one finds 2PN-accurate expressions for $d\bar{x}/dt$ and $d\bar{e}_t/dt$ that incorporate the secular effects of GW emission at 2PN order. In what follows, we explain how we adapt and improve (numerically) the GW phasing approach of Ref. [27] by employing x, e_t, c_l and c_λ to characterize 2PN-accurate eccentric orbits. Therefore, our approach parallels the x -model in some aspects, and we will highlight the differences between the two models subsequently.

Our approach to obtain $h_{+, \times}|_Q(t)$ for compact binaries that are under the influence of fully 2PN-accurate description in both conservative and reactive dynamics requires certain PN-accurate parametric expressions. These expressions provide the 2PN-accurate conservative dynamics for the variables that appear in the $h_{+, \times}|_Q(t)$. We list in a partially symbolic manner the 2PN-accurate equations for $\{r, \dot{r}, \phi, \dot{\phi}\}$ in terms of x, e_t and u as

$$\begin{aligned} \frac{\dot{r}}{c} &= \frac{\sqrt{x} e_t \sin u}{1 - e_t \cos u} \left\{ 1 + \dot{r}^{1\text{PN}}(\eta, e_t) x \right. \\ &\quad \left. + \dot{r}^{2\text{PN}}(\eta, e_t, u) x^2 \right\}, \\ \frac{r \dot{\phi}}{c} &= \frac{\sqrt{1 - e_t^2} \sqrt{x}}{1 - e_t \cos u} \left\{ 1 + r^{1\text{PN}}(\eta, e_t, u) x \right. \\ &\quad \left. + r^{2\text{PN}}(\eta, e_t, u) x^2 \right\} \times \left\{ 1 + \dot{\phi}^{1\text{PN}}(\eta, e_t, u) x \right\} \end{aligned} \quad (3.7a)$$

$$+ \dot{\phi}^{2\text{PN}}(\eta, e_t, u) x^2 \Big\}, \quad (3.7b)$$

$$\frac{Gm}{c^2 r} = \frac{x}{1 - e_t \cos u} \left\{ 1 + r^{1\text{PN}}(\eta, e_t, u) x + r^{2\text{PN}}(\eta, e_t, u) x^2 \right\}^{-1}, \quad (3.7c)$$

$$\phi = \lambda + W(\eta, x, e_t, u), \quad (3.7d)$$

where the explicit functional forms for the various PN contributions like $\dot{r}^{1\text{PN}/2\text{PN}}$ are provided in appendix B. These expressions can be easily obtained from Ref. [15] while using the 2PN-accurate relation between ω and n as given in Ref. [36].

The periodic contributions to the angular variable, given by $W(x, e_t, u)$, require additional considerations. Following Ref. [27], we write

$$W = (v - u) + e_t \sin u + W^{1\text{PN}}(\eta, e_t, u) x + W^{2\text{PN}}(\eta, e_t, u) x^2, \quad (3.8)$$

where the explicit expressions for $W^{1\text{PN}/2\text{PN}}$ are also listed in appendix B. We employ the following exact relation for the $(v - u)$ part of W [15]:

$$v - u = 2 \tan^{-1} \left[\frac{\beta_\phi \sin u}{1 - \beta_\phi \cos u} \right], \quad (3.9)$$

where $\beta_\phi = (1 - \sqrt{1 - e_\phi^2})/e_\phi$ and e_ϕ stands for a certain ‘angular eccentricity’ parameter of the PN-accurate Keplerian-type parametric solution. The higher-order PN corrections enter while connecting e_ϕ to e_t with the help of relevant expressions available in Ref. [26]. It is fairly straightforward to express β_ϕ in terms of x and e_t at 2PN order as

$$\beta_\phi = \frac{1 - \sqrt{1 - e_t^2}}{e_t} + \beta_\phi^{1\text{PN}}(\eta, e_t) x + \beta_\phi^{2\text{PN}}(\eta, e_t) x^2, \quad (3.10)$$

where the explicit expressions for the PN contributions are again listed in appendix B. In practice, we use the 2PN-accurate expression for β_ϕ while evaluating $v - u$ terms appearing in various PN orders of W .

To obtain the temporal evolution of these dynamical variables which are explicit functions of u , we solve the following 2PN-accurate Kepler equation to connect u and l . In terms of x and e_t , the 2PN-accurate KE reads

$$l = u - e_t \sin u + x^2 \left\{ \frac{(15 - 6\eta)(v - u)}{2\sqrt{1 - e_t^2}} + \frac{\eta(15 - \eta)e_t \sin u}{8(1 - e_t \sin u)} \right\}, \quad (3.11)$$

where the $v - u$ term appearing at the 2PN order on the right hand side of Eq. (3.11) is evaluated using the above prescription involving β_ϕ .

To solve the 2PN-accurate KE, we employ a modified version of Mikkola’s method for solving the classical KE, as introduced in Ref. [29]. This computationally inexpensive root-finding method involves the solution of a cubic polynomial and a subsequent fourth-order iteration to improve on the initial guess. Mikkola’s solution is valid for all l and for $0 \leq e_t \leq 1$ (see Ref. [39] for details). To solve KE at the 2PN-order, we first apply Mikkola’s method to the relation $l = u - e_t \sin(u)$ to obtain a certain ‘Newtonian’ accurate u value for a given l . This solution is employed to determine the 2PN corrections to the usual KE, namely $l_2(u, x, e_t)$. In other words, the first use of Mikkola’s method allows us to obtain the temporal variation of $l_2(u, x, e_t)$ appearing on the right-hand side of Eq. (3.11). We subsequently apply Mikkola’s method a second time to solve the ‘quasi-classical’ 2PN-accurate KE, namely $\tilde{l} = u_{2\text{PN}} - e_t \sin(u_{2\text{PN}})$, where $\tilde{l} = l - l_2(u, x, e_t)$. (More details on the implementation at the 2PN order can be found in Ref. [32].) This allows us to relate u to l (or time) at the 2PN level and therefore to describe the temporal evolution of the dynamical variables due to the conservative 2PN-accurate orbital dynamics. The use of the above semi-analytic approach ensures that the orbital time scale variations are included in a computationally inexpensive way while trying to obtain $h_{+, \times} |_{\text{Q}}(t)$.

Now let us describe how we implement the secular evolution of the two orbital elements and two angular variables that appear in the PN-accurate Keplerian description. The secular evolution of the orbital elements, namely x and e_t , arises due to the effects of GW emission. In contrast, the differential equations for l and λ are due to the conservative 2PN-accurate orbital dynamics. Additionally, the use of the above four differential equations ensures that our time-domain approximant reduces to the 2PN order TaylorT4 approximant in the circular limit. We begin by explaining the procedure to compute the differential equations for x and e_t . These two equations require two crucial inputs, and the first input involves 2PN-accurate expressions for e_t^2 and ω in terms of \mathcal{E} and \mathcal{J} in harmonic gauge, extractable from Ref. [26]. The 2PN-accurate expressions for the orbital averaged far-zone energy and angular momentum fluxes, computed in Refs. [36, 42], form the second input. We employ the energy and angular momentum balance arguments to obtain differential equations for the secular evolution of x and e_t after taking the time derivatives of the 2PN-accurate expressions for x and e_t^2 , expressed in terms of \mathcal{E} and \mathcal{J} . The resulting differential equations for the secular evolution of x and e_t may be displayed as

$$\frac{dx}{dt} = \eta \frac{c^3}{Gm} x^5 \left\{ \frac{192 + 584 e_t^2 + 74 e_t^4}{15(1 - e_t^2)^{7/2}} + \dot{x}^{1\text{PN}}(\eta, e_t) x + \dot{x}^{1.5\text{PN}}(e_t) x^{3/2} + \dot{x}^{2\text{PN}}(\eta, e_t) x^2 \right\}, \quad (3.12a)$$

$$\begin{aligned} \frac{de_t}{dt} = & -\eta e_t \frac{c^3}{Gm} x^4 \left\{ \frac{304 + 121 e_t^2}{15(1 - e_t^2)^{5/2}} \right. \\ & + \dot{e}_t^{1\text{PN}}(\eta, e_t) x + \dot{e}_t^{1.5\text{PN}}(e_t) x^{3/2} \\ & \left. + \dot{e}_t^{2\text{PN}}(\eta, e_t) x^2 \right\}, \end{aligned} \quad (3.12b)$$

where the explicit expressions for various PN contributions are listed as Eqs. (B9) in the appendix. These equations are consistent with their equivalent versions in Ref. [36].

In our approach, we have adapted a computationally efficient way to incorporate the (relative) 1.5PN corrections to \dot{x} and \dot{e}_t . These contributions are due to the dominant order tail effects that arise from the non-linear interactions between the multipole moments of the GW radiation field and the mass monopole of the source.

The tail contributions are non-local in time and therefore hereditary in nature. Following Refs. [30, 31], we write the orbital-averaged far-zone energy and angular momentum fluxes as

$$\langle \mathcal{F} \rangle_{\text{hered}} = \frac{32}{5} \frac{c^5}{G} \eta^2 x^5 [4\pi x^{3/2} \varphi(e_t)], \quad (3.13a)$$

$$\langle \mathcal{G} \rangle_{\text{hered}} = \frac{32}{5} c^2 \eta^2 m x^{7/2} [4\pi x^{3/2} \tilde{\varphi}(e_t)], \quad (3.13b)$$

where $\varphi(e_t)$ and $\tilde{\varphi}(e_t)$ define certain eccentricity enhancement functions. These functions are usually given in terms of infinite sums of Bessel functions $J_n(ne_t)$ and their derivatives w.r.t (ne_t) . The presence of infinite sums of such special functions implies that the numerical evaluation of the eccentricity enhancement functions can be computationally expensive. In this paper, we implement the e_t enhancement functions with the help of the following rational functions of e_t :

$$\begin{aligned} \varphi(e_t) = & \left(1 + 7.260831042 e_t^2 + 5.844370473 e_t^4 + 0.8452020270 e_t^6 + 0.07580633432 e_t^8 + 0.002034045037 e_t^{10} \right) / \\ & \left(1 - 4.900627291 e_t^2 + 9.512155497 e_t^4 - 9.051368575 e_t^6 + 4.096465525 e_t^8 - 0.5933309609 e_t^{10} \right. \\ & \left. - 0.05427399445 e_t^{12} - 0.009020225634 e_t^{14} \right), \end{aligned} \quad (3.14a)$$

$$\begin{aligned} \tilde{\varphi}(e_t) = & \left(1 + 1.893242666 e_t^2 - 2.708117333 e_t^4 + 0.6192474531 e_t^6 + 0.05008474620 e_t^8 - 0.01059040781 e_t^{10} \right) / \\ & \left(1 - 4.638007334 e_t^2 + 8.716680569 e_t^4 - 8.451197591 e_t^6 + 4.435922348 e_t^8 - 1.199023304 e_t^{10} \right. \\ & \left. + 0.1398678608 e_t^{12} - 0.004254544193 e_t^{14} \right). \end{aligned} \quad (3.14b)$$

The coefficients of the above two rational functions are obtained from the Taylor expanded versions of $\varphi(e_t)$ and $\tilde{\varphi}(e_t)$ in the small e_t limit. The procedure to construct such rational functions is explained in Sec. 8.3 of Ref. [23]. Invoking the terminology of Ref. [23], we may refer to the above $\varphi(e_t)$ and $\tilde{\varphi}(e_t)$ expressions as Pade approximants $P_7^5(e_t^2)$. We have verified that the numerical estimates of $\varphi(e_t)$ and $\tilde{\varphi}(e_t)$ that are based on our Eqs. (3.14) match accurately with those listed in Tables I and II in Ref. [36] for $e_t \leq 0.9$. We observe that Ref. [36] obtained these e_t enhancement functions numerically through a Fourier analysis of quasi-Keplerian motion. This gives us confidence in applying the above rational functions to compute the tail contributions to \dot{x} and \dot{e}_t . With the help of the above two rational functions, it is fairly straightforward to obtain the 1.5PN-accurate tail contributions to the differential equations for x and e_t as

$$\dot{x}^{1.5\text{PN}}(e_t) = \frac{64}{5} \left[4\pi \varphi(e_t) \right], \quad (3.15a)$$

$$\dot{e}_t^{1.5\text{PN}}(e_t) = \frac{32}{5} \left[\frac{985}{48} \pi \varphi_e(e_t) \right], \quad (3.15b)$$

where

$$\varphi_e(e_t) = \frac{192}{985} \frac{\sqrt{1 - e_t^2}}{e_t^2} \left[\sqrt{1 - e_t^2} \varphi(e_t) - \tilde{\varphi}(e_t) \right]. \quad (3.16)$$

Let us now explain why we need two additional differential equations to specify l and λ evolutions. Recall that we require to specify the values of x, e_t, l and λ at each instant to obtain the temporally evolving $h_{+, \times}|_{\text{Q}}(t)$ for compact binaries that are specified by certain values of x, e_t, c_l and c_λ at the initial epoch. Therefore, it is very convenient to provide differential equations for describing the temporal evolution of l and λ for binaries inspiraling along PN-accurate eccentric orbits. Additionally, the differential equation for λ ensures that in the circular limit our eccentric approximant goes to the **TaylorT4** approximant, as $\phi = \lambda$ in this limit. The differential equations

for l and λ are given by

$$\frac{dl}{dt} = n = x^{3/2} \frac{c^3}{Gm} \left\{ 1 + l^{1\text{PN}}(e_t) x + l^{2\text{PN}}(\eta, e_t) x^2 \right\}, \quad (3.17a)$$

$$\frac{d\lambda}{dt} = \omega = x^{3/2} \frac{c^3}{Gm}, \quad (3.17b)$$

and the PN contributions are once again listed in the appendix. It is not very difficult to deduce that the equation for \dot{l} arises from the PN-accurate relation connecting n and ω (see Ref. [36]). The differential equation for λ is due to the fact that the orbital averaged differential equation for ϕ , namely $\langle d\phi/dt \rangle$, is identical to $d\lambda/dt = \omega$. With the listing of the above two equations, we have all the ingredients to obtain $h_{+, \times}|_Q(t)$ for compact binaries inspiraling under the influence of 2PN-accurate GW emission while moving along 2PN-accurate eccentric orbits.

Observe that the e_t contributions are treated in an exact manner in all the instantaneous contributions to the differential equations for x, e_t and l that appear at the Newtonian, 1PN and 2PN orders. The use of rational functions at 1.5PN order ensures that we also have closed form expressions to evolve x and e_t . Note that it is the use of rational functions, analytic expressions for the dynamical variables and Mikkola's method that make our approach numerically accurate and possibly computationally less expensive than the x -model at this PN order. However, further investigations will be required to quantify this observation.

Let us now briefly explain the time-domain x -model, proposed in Ref. [28], to compute PN-accurate waveforms for eccentric inspirals. This model also invokes x and e_t to characterize the binary orbit. Therefore, the effects of GW emission on the usual dynamical variables are included by solving 2PN-accurate differential equations for x and e_t . Certain numerical fits are employed to model the 1.5PN order tail contributions to \dot{x} and \dot{e}_t , as detailed in Ref. [28]. However, the conservative dynamics is 3PN-accurate and the associated parametric expressions for the dynamical variables can be quite lengthy. The x -model employs PN-accurate expressions for r and $\dot{\phi}$ in terms of x, e_t and u ; hence the x -model also requires solving the PN-accurate Kepler equation to model the conservative temporal evolution of these dynamical variables. In contrast to our approach, Ref. [28] numerically differentiates and integrates the parametric expressions for r and $\dot{\phi}$ to obtain values of \dot{r} and $\dot{\phi}$ at each time step. This was pursued due to the lengthy nature of these dynamical variables. In our opinion, the use of numerical integration and differentiation at every time step to obtain $h_{+, \times}|_Q(t)$ may make the x -model computationally more demanding than our present approach. As noted earlier, further investigations involving our approach at the fully 3PN order for binaries with arbitrary η values should be pursued to clarify the above observation.

To operationalize our prescription, we choose certain (x, e_t, c_l, c_λ) values at an initial epoch to specify our (m, η, ι) binary. The use of 2PN-accurate KE results in the corresponding value for $h_{+, \times}|_Q(t)$ at that initial epoch. We numerically solve simultaneously the four differential equations for x, e_t, l and λ to obtain values of these variables at $t_0 + \Delta t$. The use of KE at that step results in unique values for $h_{+, \times}|_Q(t)$ at that instant. We repeat these steps till x reaches its cut-off value of ~ 0.1667 . This value arises as we terminate the orbital evolution when the orbital separation reaches the value associated with the last stable orbit (LSO) for a test particle in a Schwarzschild space-time, namely $r_{\text{LSO}} = 6 Gm/c^2$. This leads to the above m independent value for x . Therefore, we clearly do not include eccentricity effects on our termination value for x . Additionally, we do not consider the possibility that eccentric orbits near the LSO may not obey a Keplerian-type parametric solution as noted in Ref. [27]. We plan to investigate these subtle issues in another paper. In what follows, we display GW polarization states of our approach and probe preliminary data analysis implications.

B. Eccentric TaylorT4 approximant: facets and implications

We are now in a position to numerically implement $h_{+, \times}|_Q(t)$ that model GWs from non-spinning compact binaries inspiraling along 2PN-accurate eccentric orbits under the influence of GW emission at 2PN order. In Fig. 2, we display temporal plots for the scaled $h_{+, \times}|_Q(t)$ for $m_1 = m_2 = 10 M_\odot$ BH-BH binaries with moderate and high initial eccentricities in the aLIGO frequency window, namely $e_0 = 0.45$ and $e_0 = 0.85$, respectively. In these plots, $H_{+, \times}(t)$ stand for $h_{+, \times}|_Q(t)$ scaled by $Gm\eta/(c^2 D_L)$. The upper row of plots shows $H_{+, \times}(t)$ for binaries with $e_0 = 0.45$ while the lower row of plots depicts the GW polarization states when $e_0 = 0.85$, with $\iota = \pi/3$ in both cases. The plots for the case of moderate initial eccentricity clearly show the chirping of GW signals that are modulated by the advance of periastron. For high initial eccentricity, we observe that the GW signal consists of a series of repeated bursts; these bursts of GWs arise from the successive periastron passages. Note that the time intervals between successive peaks of GWs decrease substantially. This is due to the e_t induced shortening of the GW radiation reaction time scale. As a result, the signal duration of the $e_0 = 0.85$ inspiral in the aLIGO frequency window is substantially shorter compared to the $e_0 = 0.45$ inspiral.

Strictly speaking, our approach to model aLIGO inspirals with high e_0 values can be problematic. This is because of the possibility that the Keplerian-type parametric solution may not be appropriate to model such highly eccentric and relativistic orbits as noted in Ref. [27]. It will be desirable to adapt and extend the Effective-One-Body (EOB) formalism for general orbits, detailed in

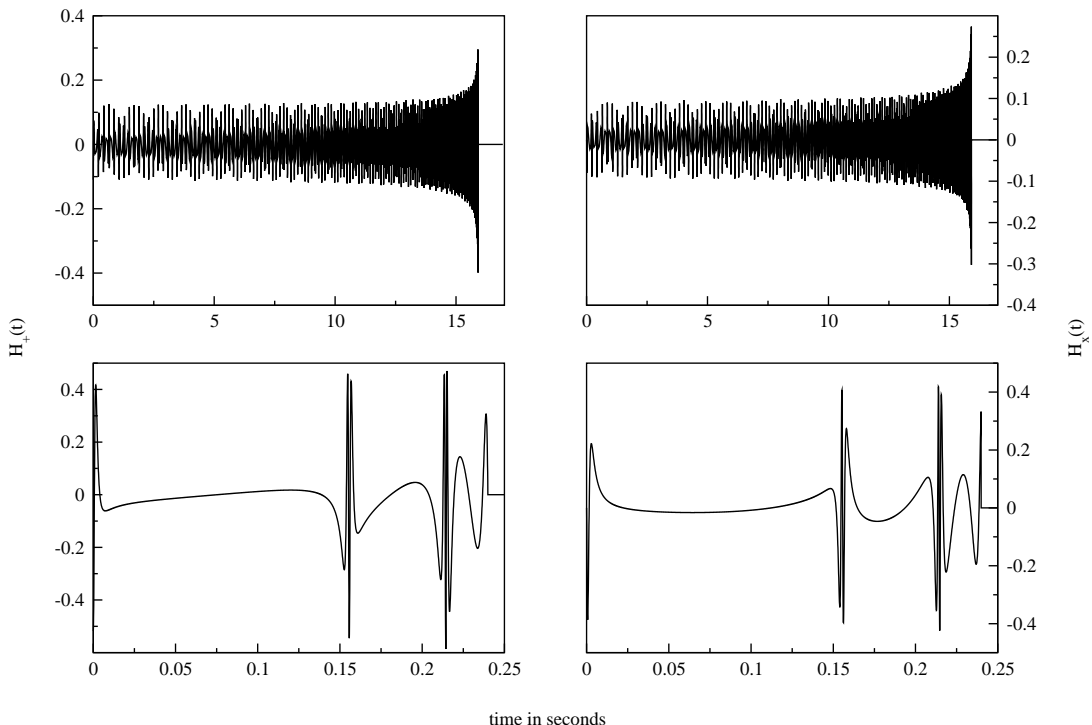


FIG. 2. Plots that display temporally evolving scaled GW polarization states $H_{+,\times}|_Q(t)$ for stellar-mass BH-BH binaries with $m_1 = m_2 = 10 M_\odot$ and for two e_0 values. The plots in the upper and lower panels consider binaries with $e_0 = 0.45$ and 0.85 , respectively. We observe chirping GW signals modulated by the influence of periastron advance in the upper panel plots. The lower panel plots depict the ‘repeated burst’ nature of highly eccentric inspirals.

Ref. [43], to model GWs from such binaries.

An important aspect of our approach is its ability to treat the eccentricity contributions in an exact manner while modeling the time-domain inspiral waveforms. In this context, the ‘exact in e_t ’ feature of our approach refers to the fact that the e_t contributions are incorporated in a non-perturbative manner. This is mainly due to the use of a PN-accurate Keplerian-type parametric solution while tackling the conservative dynamics and the use of rational functions while incorporating the tail contributions into the PN-accurate \dot{x} and \dot{e}_t expressions. Note that the instantaneous contributions to the differential equations for x and e_t , appearing at Newtonian, 1PN and 2PN order, treat e_t in an exact manner due to the use of PN-accurate Keplerian-type parametric solution for the orbital averaging [42]. This results in closed form expressions for the instantaneous contributions to \dot{x} and \dot{e}_t . Strictly speaking, our 2PN-accurate approximant treats e_t contributions in an exact manner, provided $e_0 < 0.9$, due to the use of rational functions at 1.5PN order as noted earlier. This feature allows us to employ our approximant to probe the GW data analysis implications of using inspiral templates where orbital eccentricity effects are treated in an approximate manner, especially while incorporating the effects of GW emission. For this purpose, we construct a second time-domain inspiral family, namely a Te8 approximant, by

Taylor expanding the differential equations for x and e_t , given by Eqs. (3.12a) and (3.12b), in the small e_t limit while keeping e_t contributions accurate up to $\mathcal{O}(e_t^8)$. This Te8 approximant is motivated by our observations that one will be forced to treat e_t in an approximate manner if one wishes to incorporate effects of orbital eccentricity into other circular time domain approximants like **TaylorT1**, **T2**, and **T3** in a straightforward manner. We are restricting e_t contributions to the eighth order to be consistent with the order of eccentricity corrections available in the PC and EPC prescriptions [10, 14]. The match (\mathcal{M}) estimates, detailed in Refs. [17, 44], are invoked to compare the e_t exact and e_t truncated waveform families. In particular, we explore the faithfulness of the e_t truncated waveform family. Faithfulness requires that the associated match (\mathcal{M}) values are greater than 0.97. A few comments are in order before we proceed with the match computations. It should be clear that the \mathcal{M} estimates between the above two approximants probe only the consequence of truncating e_t contributions while constructing time-domain inspiral waveform families. At present, we do not explicitly pursue match computations between our 2PN order eccentric extension of the **TaylorT4** model and the various Fourier-domain models, available in Refs. [10, 14] and in the previous section. This is mainly due to the model-dependent systematic mismatch that occurs while comparing even the

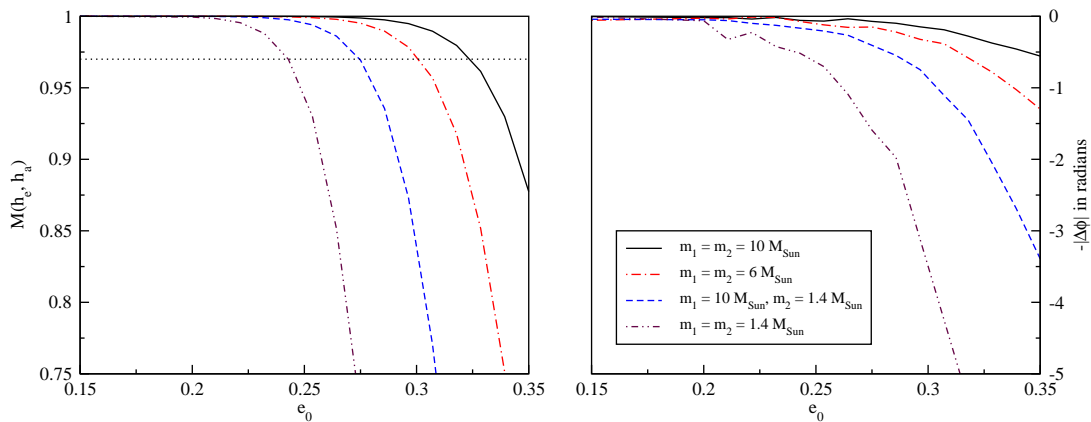


FIG. 3. (Color Online) Plots that probe the total-mass dependence of our $\mathcal{M}(h_e, h_a)$ and the related $|\Delta\phi(h_e, h_a)|$ estimates as functions of e_0 for a number of aLIGO relevant stellar-mass compact binaries. The h_e inspiral waveforms are based on our eccentric **TaylorT4** approximant while h_a waveforms arise from the Te8 approximant, as detailed in the text. The critical e_0 values are higher for higher mass binaries due to their shorter inspiral lifespan in the aLIGO frequency window. A clear correlation exists between the drop in the $\mathcal{M}(h_e, h_a)$ values and their associated $\Delta\phi(h_e, h_a)$ values.

time-domain and frequency-domain quasi-circular inspiral templates [9]. Therefore, it is reasonable to expect similar systematic effects when considering eccentric inspiral templates in the time and frequency domain. However, we would like to emphasize that in the $e_0 \rightarrow 0$ limit our fully analytic frequency-domain waveforms $\tilde{h}(f)$ reduce to the **TaylorF2** model at 2PN order exactly. Finally, in the following (see Figs. 3 and 4) h_e stands for our eccentric extension of the **TaylorT4** approximant where e_t contributions are treated in an exact manner while h_a stands for time domain waveform families based on the truncated Te8 approximant.

The $\mathcal{M}(h_e, h_a)$ computations that we pursue here require us to define a certain overlap function between our time domain h_e and h_a inspiral waveform families where h_e and h_a refer to the respective cross polarization states of the GW. The overlap integral $\mathcal{O}(h_e, h_a)$ is defined as

$$\mathcal{O}(h_e, h_a) = \frac{\langle h_e | h_a \rangle}{\sqrt{\langle h_e | h_e \rangle \langle h_a | h_a \rangle}}. \quad (3.18)$$

Clearly, the overlap integral requires a certain normalized inner product involving the $h_e(t)$ and $h_a(t)$ families. This is given by

$$\langle h_e | h_a \rangle = 4 \operatorname{Re} \int_{f_{\text{low}}}^{f_{\text{cut}}} \frac{\tilde{h}_e^*(f) \tilde{h}_a(f)}{S_h(f)} df. \quad (3.19)$$

The symbols $\tilde{h}_e(f)$ and $\tilde{h}_a(f)$ stand for the Fourier transforms of the $h_e(t)$ and $h_a(t)$ inspiral waveforms while $S_h(f)$ denotes the one-sided power spectral density of the detector noise. We have used the zero-detuned, high power (ZDHP) noise configuration of aLIGO, provided in Ref. [45], for the present $\mathcal{M}(h_e, h_a)$ computations. For these match estimates, we let f_{low} be 10 Hz, corresponding to the lower cut-off frequency of aLIGO, while the upper cut-off frequency, as noted earlier, is chosen to

be $f_{\text{LSO}} = c^3/(Gm\pi 6^{3/2})$. The match $\mathcal{M}(h_e, h_a)$ is obtained by maximizing the above overlap over certain kinematical variables of h_e such that

$$\mathcal{M}(h_e, h_a) = \max_{t_0, \phi_0} \mathcal{O}(h_e, h_a), \quad (3.20)$$

where t_0 and ϕ_0 are the detector arrival time and the associated phase ϕ_0 of the h_e template. The maximization over t_0 is performed with the help of the FFT algorithm, while we apply two orthogonal templates to maximize over ϕ_0 [17]. In our match estimates, all other parameters pertaining to both h_e and h_a waveform families are treated to be identical. Let us emphasize that $\mathcal{M}(h_e, h_a) > 0.97$ implies that the approximate Te8 waveform family will recover our time-domain approximant, constructed to be an eccentric extension of the 2PN-accurate **TaylorT4** approximant, in a ‘faithful’ manner.

In Fig. 3, we plot the $\mathcal{M}(h_e, h_a)$ estimates and the absolute values of the related accumulated phase differences, namely $|\Delta\phi|$, as functions of e_0 for typical aLIGO relevant compact binaries containing NSs and BHs. The plots indicate that $\mathcal{M}(h_e, h_a)$ values drop below 0.97 when $|\Delta\phi(h_e, h_a)|$ values are ~ 0.5 radians. A direct correlation between the drop in $\mathcal{M}(h_e, h_a)$ values and their $-|\Delta\phi(h_e, h_a)|$ values is also observed. The critical values e_0^c for initial eccentricity, above which the $\mathcal{M} \leq 0.97$, lie roughly in the 0.25 – 0.35 range for our aLIGO binaries. These e_0^c values clearly depend on the total mass m , and we observe that the $\{h_e, h_a\}$ templates with higher total mass dephase at higher e_0 values compared to their lower mass counterparts. A possible explanation is that the lower mass binaries last longer in the aLIGO frequency window which provides more time for even small differences between the two approximants to grow. For higher mass binaries, comparable changes in $|\Delta\phi(h_e, h_a)|$ values

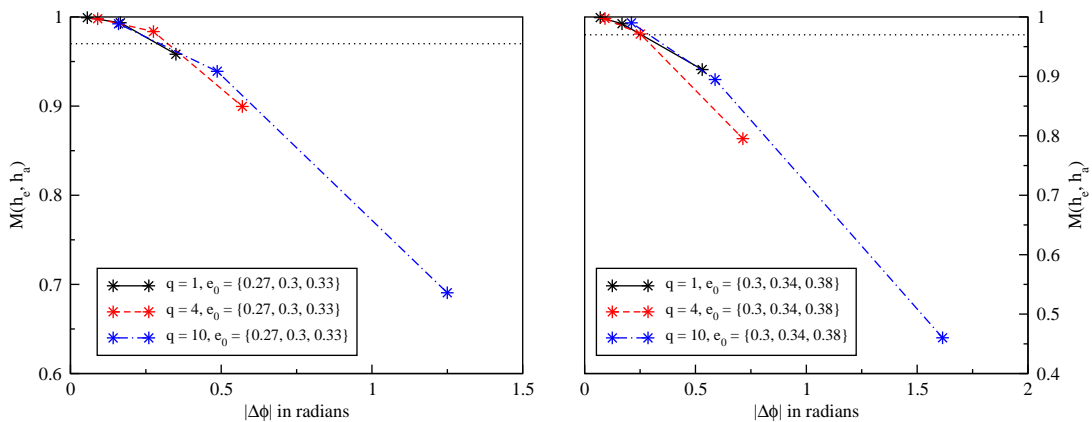


FIG. 4. (Color Online) Plots that probe the dependence of our $\mathcal{M}(h_e, h_a)$ estimates on the mass ratio q . We display a set of $\{\mathcal{M}(h_e, h_a), |\Delta\phi(h_e, h_a)|\}$ values for BH-BH binaries with different q and e_0 values. The left panel considers binaries with $m = 20 M_\odot$, while the right panel contains data points for binaries with $m = 40 M_\odot$. Sharper drops in the match estimates are clearly visible for binaries with larger q . The neglected orbital eccentricity contributions in the h_a waveforms force them to dephase strongly from their h_e counterparts during the comparatively longer aLIGO evolution window for the binaries with larger q .

occur for higher e_0 values due to their shorter lifespan in the aLIGO band. This is also clearly evident while comparing the plots for the NS-NS and BH-BH binaries. The observed direct correlation between the drop in $\mathcal{M}(h_e, h_a)$ values and their $-|\Delta\phi(h_e, h_a)|$ values has direct implications for our $\tilde{h}(f)$ computations, detailed in Sec. II, and the numbers listed in Table I. This correlation implies that match computations between our 2PN order $\tilde{h}(f)$ and its EPC counterpart should yield \mathcal{M} values substantially lower than 0.97 for configurations with $e_0 \sim 0.1$. Therefore, including the effects of orbital eccentricity evolution into $\tilde{h}(f)$ in a PN-accurate manner is also important from the perspective of match computations.

Let us move on to probe the influence of the mass ratio $q = m_1/m_2$ on our $\mathcal{M}(h_e, h_a)$ estimates. In Fig. 4, we display a set of $\{\mathcal{M}(h_e, h_a), |\Delta\phi(h_e, h_a)|\}$ values for BH-BH binaries with different q and e_0 values. The plots in the left and right panels consider binaries with total mass $m = 20 M_\odot$ and $40 M_\odot$, respectively. The e_0 values have been chosen so that the maximum $|\Delta\phi(h_e, h_a)|$ value will not exceed two radians. We observe a sharp drop in $\mathcal{M}(h_e, h_a)$ values for binaries with larger q . This may also be related to the fact that such binaries last longer in the aLIGO frequency window compared to their counterparts with lower q value. The neglected orbital eccentricity contributions force the e_t truncated h_a templates to dephase strongly from their e_t exact h_e counterparts during the comparatively longer aLIGO evolution window for the binaries with larger q . This dephasing provides a natural explanation for the sharp drop in the $\mathcal{M}(h_e, h_a)$ estimates for such binaries, as is evident from the plots for binary configurations with smaller m and larger q .

We probe the ability of the 2PN-accurate quasi-circular

TaylorT4 approximant to faithfully capture its eccentric extension in Fig. 5. We plot $\mathcal{M}(h_e, h_a)$ estimates and the related $|\Delta\phi(h_e, h_a)|$ as functions of e_0 , where h_a now stands for inspiral templates based on the quasi-circular 2PN-accurate **TaylorT4** approximant. The quasi-circular templates can faithfully capture an eccentric GW signal only if the binary has a tiny residual eccentricity when the system enters the aLIGO band. The e_0^c value above which the match estimates fall below 0.97 is again m dependent. This critical initial eccentricity is ~ 0.04 for BH-BH binaries with $m = 20 M_\odot$, while $e_0^c \sim 0.005$ for NS-NS binaries. For low mass binaries, the neglected eccentricity contributions force the h_a templates to dephase strongly from their h_e counterparts, due to the comparatively longer inspiral time of such binaries in the aLIGO window. This provides the expected explanation for the m dependency of the critical e_0^c values. These observations are consistent with the fitting factor calculations that probed the ability of the quasi-circular **TaylorT4** approximant to detect GWs from eccentric binaries constructed with the help of the x -model [22].

Finally, we invoke the above match plots and the 2PN *analytic* entries of Table. I to provide a non-rigorous justification for truncating our frequency-domain approximant to $\mathcal{O}(e_0)^6$. The match plots of the present section reveal that our approximate time domain waveform family with eccentricity contributions accurate up to $\mathcal{O}(e_0)^8$ is faithful to our *exact in e_t* time-domain approximant only for initial eccentricities $e_0 \leq 0.25 - 0.35$, depending on the total mass of the binary. We have also checked that the fractional differences in \mathcal{N} , associated with the 2PN *analytic* entries, are also fairly constant while considering initial eccentricities up to 0.25. This suggests that including eccentricity contributions accu-

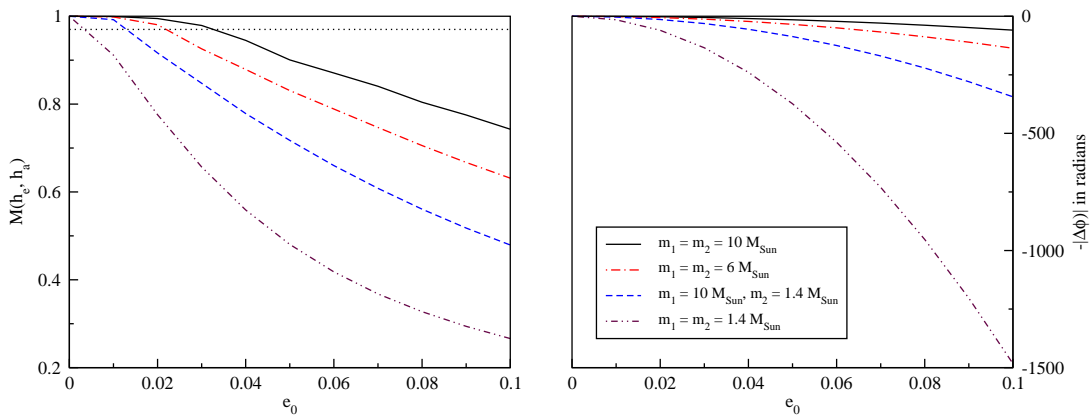


FIG. 5. (Color Online) Plots that probe the faithfulness of the quasi-circular 2PN TaylorT4 approximant with respect to its eccentric extension. The $\mathcal{M}(h_e, h_a)$ estimates and the related $|\Delta\phi(h_e, h_a)|$ as functions of e_0 are considered for typical aLIGO binaries. Clearly, the quasi-circular templates are faithful to our eccentric TaylorT4 approximant only for binaries with tiny residual eccentricities like 10^{-2} or less. Hence, such templates can capture an eccentric GW signal only if the binary has a tiny residual eccentricity when the system enters the aLIGO band.

rate to $\mathcal{O}(e_0)^6$ is sufficient from the point of view of accumulated number of GW cycles \mathcal{N} . Therefore, it may be reasonable to expect that *approximate in eccentricity* frequency-domain inspiral families are also faithful to our e_t exact time-domain approximant only up to such initial e_0 values. Additionally, we observe that the *2PN analytic* \mathcal{N} estimates do not change substantially when we drop the $\mathcal{O}(e_0)^6$ contributions to $\phi(x, e_0, F_0)$ for binaries with initial eccentricities up to 0.25. These considerations, in our opinion, provide reasonable justification for restricting the initial eccentricity corrections up to $\mathcal{O}(e_0)^6$ at each PN order in our frequency-domain approximant and therefore to let the harmonic index j vary up to 8 in Eq. (2.14). Clearly, match estimates involving frequency and time domain waveform families that are accurate to 3PN order will be desirable to check the validity of these statements. We expect that this extension should also clarify the need to go beyond the $\mathcal{O}(e_0)^6$ corrections from the point of view of the lengthy expressions for Ψ_j and $e_t(\omega)$.

IV. CONCLUSIONS

In this paper, we computed a fully analytic frequency-domain inspiral waveform with Newtonian amplitude and 2PN order Fourier phase while incorporating eccentricity effects up to sixth order at each PN order. This is achieved by extending the post-circular scheme of Ref. [14] by incorporating the effects of PN-accurate orbital eccentricity evolution. With the help of the accumulated number of GW cycles in a certain $x_{\text{low}} - x_{\text{high}}$ window, suitable for the advanced GW detectors, we showed the importance of incorporating eccentric contributions to the Fourier phase in a PN consistent manner. We also presented a prescription to incorporate orbital eccentric-

ity into the quasi-circular time domain TaylorT4 approximant at 2PN order. This involved employing rational functions in orbital eccentricity to implement the 1.5PN order tail contributions to the far-zone fluxes and a modified version of Mikkola's method to solve the PN-accurate Kepler equation. Our approach contains closed form PN-accurate differential equations for evolving PN-accurate eccentric orbits while treating eccentricity effects in an exact manner. We point out that our time domain eccentric approximant should be accurate and efficient to handle initial orbital eccentricities ≤ 0.9 . With the help of match estimates, preliminary GW data analysis implications are probed. We note in passing that the above prescriptions for eccentric inspiral templates have been implemented in the LSC Algorithm Library of the LIGO Scientific Collaboration.

A number of extensions are possible and some of these are being actively pursued. Indeed, it is possible to extend the PN-accuracy of both approximants to the next PN order. For the frequency-domain waveforms, we require 3PN-accurate expressions for $\dot{\omega}$ and \dot{e}_t , available in Ref. [36]. At present, efforts are on-going to extend the analysis of Ref. [37] by incorporating e_0^2 contributions to the SPA phase at 3PN order [46]. It should also be possible to include the effect of periastron advance by adapting and extending the arguments present in Sec. VI of Ref. [14]. Another direction of investigation will be to incorporate PN order amplitude contributions to our $\tilde{h}(f)$ with the help of Refs. [47, 48]. In comparison, we will require the 3PN-accurate Keplerian-type parametric solution of Ref. [26] and the 3PN-accurate $\dot{\omega}$ and \dot{e}_t expressions of Ref. [36] to extend our e_t exact time-domain approximant to the next PN order. This extension should allow us to estimate the comparative accuracies and efficiencies of the x -model and our fully 3PN-accurate time-domain approximant while consider-

ing compact binaries with arbitrary (but allowed) η and e_0 values. It should be possible to improve Ref. [49] to include the dominant order spin-orbit interactions in our time domain approximant. These PN extensions should allow one to pursue detailed comparisons with numerical relativity based eccentric inspirals, thereby extending the earlier comparison of Ref. [28]. In this context, it will be interesting to compare our PN-accurate $h(t)$ with the Effective-One-Body (EOB) based eccentric $h(t)$ family. This requires adapting the formalism of Ref. [43] to obtain the EOB based $h(t)$ during the inspiral phase.

It will also be of interest to compare our $h(t)$ with the time domain waveforms based on the `CBwaves` software, discussed in Ref. [50], while considering non-spinning compact binaries in inspiraling eccentric orbits. `CBwaves` numerically integrates 3.5PN-accurate equations of motion to incorporate the dynamics of inspiraling eccentric compact binaries into the GW polarization states. A similar approach was employed to model GWs from dynamically formed highly eccentric binaries that can last

minutes to days before coalescence [51]. Clearly, PN extensions of our $h(t)$ will be useful to obtain accurate GW templates for such a ‘repeated bursts’ scenario and to probe its implications. A possible comparison of our $h(t)$ in the small η limit with the GW strain of Ref. [52] should be helpful to mark the η range of these two approaches. The present approach, capable of modeling highly eccentric inspirals, should be interesting to various non-optimal excess power methods to search for GW bursts [53–55]. A post-Newtonian accurate analytic approach to describe the evolution of ω and e_t should be useful for the seedless clustering approach of Ref. [55].

V. ACKNOWLEDGEMENTS

We thank K. G. Arun, M. Favata, A. Gupta and E. A. Huerta for helpful discussions and suggestions. Additional thanks to K. G. Arun for providing us the numerical values for the eccentricity enhancement functions.

Appendix A: Explicit 2PN order Ψ_j , e_t and ϕ expressions

We list below the main and lengthy results of our Sec. II. Invoking the convention and symbols of Sec. II,

we write the analytic frequency-domain GW strain for eccentric inspirals with Newtonian amplitude and 2PN order phase as

$$\tilde{h}(f) = \tilde{\mathcal{A}} \left(\frac{Gm\pi f}{c^3} \right)^{-7/6} \sum_{j=1}^8 \xi_j \left(\frac{j}{2} \right)^{2/3} e^{-i(\pi/4 + \Psi_j)}, \quad (\text{A1})$$

where $\tilde{\mathcal{A}}$ and ξ_j are defined as

$$\tilde{\mathcal{A}} = - \left(\frac{5\eta\pi}{384} \right)^{1/2} \frac{G^2 m^2}{c^5 D_L}, \quad (\text{A2a})$$

$$\xi_j = \frac{(1 - e_t^2)^{7/4}}{\left(1 + \frac{73}{24}e_t^2 + \frac{37}{96}e_t^4\right)^{1/2}} \alpha_j e^{-i\phi_j(f/j)}. \quad (\text{A2b})$$

We do not list explicitly the coefficients ξ_j as polynomials in e_t while incorporating e_t contributions up to $\mathcal{O}(e_t^6)$ as required. Clearly, it is fairly straightforward to

obtain such ξ_j expressions from its above definition. The explicit expression for the 2PN-order Fourier phase Ψ_j that includes all $\mathcal{O}(e_0^6)$ contributions is given by

$$\Psi_j \sim j\phi_c - 2\pi f t_c - \frac{3}{128\eta} \left(\frac{Gm\pi f}{c^3} \right)^{-5/3} \left(\frac{j}{2} \right)^{8/3} \sum_{n=0}^4 \mathcal{C}_n x^{n/2}, \quad (\text{A3})$$

where the coefficients \mathcal{C}_n can be listed as

$$\begin{aligned} \mathcal{C}_0 = & 1 - \frac{2355}{1462} e_0^2 \chi^{-19/9} + \left(-\frac{2608555}{444448} \chi^{-19/9} + \frac{5222765}{998944} \chi^{-38/9} \right) e_0^4 + \left(-\frac{1326481225}{10134144} \chi^{-19/9} \right. \\ & \left. + \frac{173355248095}{455518464} \chi^{-38/9} - \frac{75356125}{3326976} \chi^{-19/3} \right) e_0^6, \end{aligned} \quad (\text{A4a})$$

$$\mathcal{C}_1 = 0, \quad (\text{A4b})$$

$$\begin{aligned} \mathcal{C}_2 = & \frac{3715}{756} + \frac{55}{9}\eta + \left\{ \left(-\frac{2045665}{348096} - \frac{128365}{12432}\eta \right) \chi^{-19/9} + \left(-\frac{2223905}{491232} + \frac{154645}{17544}\eta \right) \chi^{-25/9} \right\} e_0^2 \\ & + \left\{ \left(-\frac{6797744795}{317463552} - \frac{426556895}{11337984}\eta \right) \chi^{-19/9} + \left(-\frac{14275935425}{416003328} + \frac{209699405}{4000032}\eta \right) \chi^{-25/9} \right. \\ & \left. + \left(\frac{198510270125}{10484877312} + \frac{1222893635}{28804608}\eta \right) \chi^{-38/9} + \left(\frac{14796093245}{503467776} - \frac{1028884705}{17980992}\eta \right) \chi^{-44/9} \right\} e_0^4 \\ & + \left\{ \left(-\frac{3456734032025}{72381689856} - \frac{216909251525}{2585060352}\eta \right) \chi^{-19/9} + \left(-\frac{2441897241139735}{21246121967616} + \frac{9479155594325}{58368466944}\eta \right) \chi^{-25/9} \right. \\ & \left. + \left(\frac{659649627625375}{4781104054272} + \frac{4063675549105}{13134901248}\eta \right) \chi^{-38/9} + \left(\frac{1968906345873305}{5969113952256} - \frac{8999675405695}{16398664704}\eta \right) \chi^{-44/9} \right. \\ & \left. + \left(-\frac{144936872901}{1691582464} - \frac{7378552295}{32530432}\eta \right) \chi^{-19/3} + \left(-\frac{213483902125}{1117863936} + \frac{14845156625}{39923712}\eta \right) \chi^{-7} \right\} e_0^6, \end{aligned} \quad (\text{A4c})$$

$$\begin{aligned}
C_3 = & -16\pi + \left(\frac{65561\pi}{4080} \chi^{-19/9} - \frac{295945\pi}{35088} \chi^{-28/9} \right) e_0^2 + \left(\frac{217859203\pi}{3720960} \chi^{-19/9} \right. \\
& - \frac{3048212305\pi}{64000512} \chi^{-28/9} - \frac{6211173025\pi}{102085632} \chi^{-38/9} + \frac{1968982405\pi}{35961984} \chi^{-47/9} \left. \right) e_0^4 + \left(\frac{22156798877\pi}{169675776} \chi^{-19/9} \right. \\
& - \frac{126468066221755\pi}{846342770688} \chi^{-28/9} - \frac{20639727962075\pi}{46551048192} \chi^{-38/9} + \frac{33366234820475\pi}{65594658816} \chi^{-47/9} \\
& \left. + \frac{30628811474315\pi}{97254162432} \chi^{-19/3} - \frac{28409259125\pi}{79847424} \chi^{-22/3} \right) e_0^6, \tag{A4d}
\end{aligned}$$

$$\begin{aligned}
C_4 = & \frac{15293365}{508032} + \frac{27145}{504} \eta + \frac{3085}{72} \eta^2 + \left\{ \left(-\frac{111064865}{14141952} - \frac{165068815}{4124736} \eta - \frac{10688155}{294624} \eta^2 \right) \chi^{-19/9} + \left(-\frac{5795368945}{350880768} \right. \right. \\
& \left. \left. + \frac{4917245}{1566432} \eta + \frac{25287905}{447552} \eta^2 \right) \chi^{-25/9} + \left(\frac{936702035}{1485485568} + \frac{3062285}{260064} \eta - \frac{14251675}{631584} \eta^2 \right) \chi^{-31/9} \right\} e_0^2 \\
& + \left\{ \left(-\frac{369068546395}{12897460224} - \frac{548523672245}{3761759232} \eta - \frac{35516739065}{268697088} \eta^2 \right) \chi^{-19/9} + \left(-\frac{37202269351825}{297145884672} \right. \right. \\
& - \frac{2132955527705}{74286471168} \eta + \frac{34290527545}{102041856} \eta^2 \left. \right) \chi^{-25/9} + \left(-\frac{94372278903235}{7251965779968} + \frac{126823556396665}{733829870592} \eta \right. \\
& - \frac{20940952805}{93768192} \eta^2 \left. \right) \chi^{-31/9} + \left(\frac{418677831611033}{34573325230080} + \frac{2163514670909}{12862100160} \eta + \frac{203366083643}{1130734080} \eta^2 \right) \chi^{-38/9} \\
& + \left(\frac{562379595264125}{5284378165248} + \frac{2965713234395}{94363895808} \eta - \frac{240910046095}{518482944} \eta^2 \right) \chi^{-44/9} + \left(\frac{3654447011975}{98224939008} \right. \\
& \left. - \frac{4300262795285}{18124839936} \eta + \frac{392328884035}{1294631424} \eta^2 \right) \chi^{-50/9} \left. \right\} e_0^4 \\
& + \left\{ \left(-\frac{187675742904025}{2940620931072} - \frac{278930807554775}{857681104896} \eta - \frac{18060683996675}{61262936064} \eta^2 \right) \chi^{-19/9} \right. \\
& + \left(-\frac{6363444229039638215}{15175834621968384} - \frac{39088433492776445}{270997046820864} \eta + \frac{1550053258427425}{1488994762752} \eta^2 \right) \chi^{-25/9} \\
& + \left(-\frac{387035983120116605285}{5846592827536441344} + \frac{1095104635088909345}{1338505683959808} \eta - \frac{185468261986684025}{191215097708544} \eta^2 \right) \chi^{-31/9} \\
& + \left(\frac{1391266434443462659}{15765436304916480} + \frac{7189359251430607}{5865117672960} \eta + \frac{675785495945689}{515614740480} \eta^2 \right) \chi^{-38/9} \\
& + \left(\frac{74835480932061169625}{62651587527180288} + \frac{14868442349448515}{21514968244224} \eta - \frac{2107245064767505}{472856444928} \eta^2 \right) \chi^{-44/9} \\
& + \left(\frac{43949506831840859555}{63177102070677504} - \frac{1344731894414361455}{376054178992128} \eta + \frac{7946157848161165}{2066231752704} \eta^2 \right) \chi^{-50/9} \\
& + \left(-\frac{984783138418096685}{40879050017734656} - \frac{258954290041765}{271268315136} \eta - \frac{173415564792655}{148551696384} \eta^2 \right) \chi^{-19/3} \\
& + \left(-\frac{136868720309511}{189457235968} - \frac{17969188685519}{35523231744} \eta + \frac{1453574802115}{390365184} \eta^2 \right) \chi^{-7} \\
& \left. + \left(-\frac{26945014260125}{52819070976} + \frac{17350371000625}{6707183616} \eta - \frac{357715525375}{119771136} \eta^2 \right) \chi^{-23/3} \right\} e_0^6. \tag{A4e}
\end{aligned}$$

The frequency dependence of e_t due to 2PN-accurate GW induced e_t evolution is given by

$$e_t \sim \sum_{n=0}^4 \mathcal{D}_n x^{n/2}. \quad (\text{A5})$$

The coefficients \mathcal{D}_n that incorporate all the $\mathcal{O}(e_0^5)$ contributions read

$$\mathcal{D}_0 = e_0 \chi^{-19/18} + \frac{3323}{1824} e_0^3 \left(\chi^{-19/18} - \chi^{-19/6} \right) + \left(\frac{15994231}{6653952} \chi^{-19/18} - \frac{11042329}{1108992} \chi^{-19/6} + \frac{50259743}{6653952} \chi^{-95/18} \right) e_0^5, \quad (\text{A6a})$$

$$\mathcal{D}_1 = 0, \quad (\text{A6b})$$

$$\begin{aligned} \mathcal{D}_2 = & \left\{ \left(\frac{2833}{2016} - \frac{197}{72} \eta \right) \left(-\chi^{-19/18} + \chi^{-31/18} \right) \right\} e_0 + \left\{ \left(-\frac{9414059}{3677184} + \frac{654631}{131328} \eta \right) \chi^{-19/18} \right. \\ & + \left(\frac{386822573}{47803392} - \frac{1482433}{131328} \eta \right) \chi^{-31/18} + \left(\frac{11412055}{5311488} - \frac{378697}{43776} \eta \right) \chi^{-19/6} \\ & + \left. \left(-\frac{9414059}{1225728} + \frac{654631}{43776} \eta \right) \chi^{-23/6} \right\} e_0^3 + \left\{ \left(-\frac{45311656423}{13414367232} + \frac{3150863507}{479084544} \eta \right) \chi^{-19/18} \right. \\ & + \left(\frac{3061519891285}{174386774016} - \frac{11147601665}{479084544} \eta \right) \chi^{-31/18} + \left(\frac{37922258765}{3229384704} - \frac{1258410131}{26615808} \eta \right) \chi^{-19/6} \\ & + \left(-\frac{699589093187}{9688154112} + \frac{3092267495}{26615808} \eta \right) \chi^{-23/6} + \left(-\frac{1182747028465}{174386774016} + \frac{24493152461}{479084544} \eta \right) \chi^{-95/18} \\ & + \left. \left(\frac{711929259595}{13414367232} - \frac{49505846855}{479084544} \eta \right) \chi^{-107/18} \right\} e_0^5, \quad (\text{A6c}) \end{aligned}$$

$$\begin{aligned} \mathcal{D}_3 = & \left\{ \frac{377\pi}{144} \left(-\chi^{-19/18} + \chi^{-37/18} \right) \right\} e_0 + \left(-\frac{1252771\pi}{262656} \chi^{-19/18} + \frac{1315151\pi}{131328} \chi^{-37/18} + \frac{396797\pi}{43776} \chi^{-19/6} \right. \\ & - \left. \frac{1252771\pi}{87552} \chi^{-25/6} \right) e_0^3 + \left(-\frac{6029825087\pi}{958169088} \chi^{-19/18} + \frac{607032981553\pi}{27786903552} \chi^{-37/18} + \frac{1318556431\pi}{26615808} \chi^{-19/6} \right. \\ & - \left. \frac{1422200801\pi}{13307904} \chi^{-25/6} - \frac{1586634546601\pi}{27786903552} \chi^{-95/18} + \frac{94739615555\pi}{958169088} \chi^{-113/18} \right) e_0^5, \quad (\text{A6d}) \end{aligned}$$

$$\begin{aligned} \mathcal{D}_4 = & \left\{ \left(\frac{77006005}{24385536} - \frac{1143767}{145152} \eta + \frac{43807}{10368} \eta^2 \right) \chi^{-19/18} + \left(-\frac{8025889}{4064256} + \frac{558101}{72576} \eta - \frac{38809}{5184} \eta^2 \right) \chi^{-31/18} \right. \\ & + \left. \left(-\frac{28850671}{24385536} + \frac{27565}{145152} \eta + \frac{33811}{10368} \eta^2 \right) \chi^{-43/18} \right\} e_0 + \left\{ \left(\frac{255890954615}{44479217664} - \frac{3800737741}{264757248} \eta \right. \right. \\ & + \left. \frac{145570661}{18911232} \eta^2 \right) \chi^{-19/18} + \left(-\frac{1095868349309}{96371638272} + \frac{65400285919}{1720922112} \eta - \frac{292039301}{9455616} \eta^2 \right) \chi^{-31/18} \\ & + \left(-\frac{20952382669619}{4047608807424} - \frac{385200824731}{24092909568} \eta + \frac{4301644427}{132378624} \eta^2 \right) \chi^{-43/18} + \left(\frac{8180980796033}{1349202935808} \right. \\ & + \left. \frac{14604819923}{2676989952} \eta - \frac{317361763}{14708736} \eta^2 \right) \chi^{-19/6} + \left(\frac{32330351815}{3569319936} - \frac{10345778159}{191213568} \eta + \frac{74603309}{1050624} \eta^2 \right) \chi^{-23/6} \\ & + \left. \left(-\frac{9164199307}{2118057984} + \frac{1205846917}{29417472} \eta - \frac{13714021}{233472} \eta^2 \right) \chi^{-9/2} \right\} e_0^3 \end{aligned}$$

$$\begin{aligned}
& + \left\{ \left(\frac{1231651832357155}{162260186038272} - \frac{18293673608177}{965834440704} \eta + \frac{700659277417}{68988174336} \eta^2 \right) \chi^{-19/18} \right. \\
& + \left(-\frac{8673285852010405}{351563736416256} + \frac{506837220151715}{6277923864576} \eta - \frac{2196077528005}{34494087168} \eta^2 \right) \chi^{-31/18} \\
& + \left(-\frac{4719697288288984795}{191953800083275776} - \frac{4676818769915975}{87890934104064} \eta + \frac{669607180808035}{6277923864576} \eta^2 \right) \chi^{-43/18} \\
& + \left(\frac{27185399185217659}{820315384971264} + \frac{48531816604129}{1627609890816} \eta - \frac{1054593138449}{8942911488} \eta^2 \right) \chi^{-19/6} \\
& + \left(\frac{2402572738143295}{28211904774144} - \frac{55792908667709}{116257849344} \eta + \frac{352402173805}{638779392} \eta^2 \right) \chi^{-23/6} \\
& + \left(-\frac{25186092424407371}{273438461657088} + \frac{936816311138573}{1627609890816} \eta - \frac{1951606822255}{2980970496} \eta^2 \right) \chi^{-9/2} \\
& + \left(-\frac{7937050519029473999}{191953800083275776} - \frac{1089957759112387}{87890934104064} \eta + \frac{1121044759543031}{6277923864576} \eta^2 \right) \chi^{-95/18} \\
& + \left(-\frac{16753611658206725}{351563736416256} + \frac{2837648691484435}{6277923864576} \eta - \frac{24125755174085}{34494087168} \eta^2 \right) \chi^{-107/18} \\
& + \left. \left(\frac{16633441088056655}{162260186038272} - \frac{79153315354555}{137976348672} \eta + \frac{47507268174605}{68988174336} \eta^2 \right) \chi^{-119/18} \right\} e_0^5. \tag{A6e}
\end{aligned}$$

This expression for e_t , as expected, is required while operationalizing the ξ_j coefficients and therefore $\dot{h}(f)$ and the parameter x in the above two expressions should be evaluated at the stationary point.

We list below the 2PN order expression for ϕ that is required to compute the accumulated number of GW cy-

cles, denoted by ‘2PN analytic’ in Table. I, as

$$\phi \sim \left(\frac{-1}{32\eta} \right) \sum_{n=-5}^{-1} \mathcal{E}_n x^{n/2}, \tag{A7}$$

where the coefficients \mathcal{E}_n are given by

$$\begin{aligned}
\mathcal{E}_{-5} = & 1 - \frac{785}{272} e_0^2 \chi^{-19/9} + \left(-\frac{2608555}{248064} \chi^{-19/9} + \frac{5222765}{386688} \chi^{-38/9} \right) e_0^4 + \left(-\frac{1326481225}{56558592} \chi^{-19/9} \right. \\
& \left. + \frac{173355248095}{176329728} \chi^{-38/9} - \frac{226068375}{2957312} \chi^{-19/3} \right) e_0^6, \tag{A8a}
\end{aligned}$$

$$\mathcal{E}_{-4} = 0, \tag{A8b}$$

$$\begin{aligned}
\mathcal{E}_{-3} = & \frac{3715}{1008} + \frac{55}{12} \eta + \left\{ \left(-\frac{2045665}{225792} - \frac{128365}{8064} \eta \right) \chi^{-19/9} + \left(-\frac{2223905}{274176} + \frac{154645}{9792} \eta \right) \chi^{-25/9} \right\} e_0^2 \\
& + \left\{ \left(-\frac{6797744795}{205922304} - \frac{426556895}{7354368} \eta \right) \chi^{-19/9} + \left(-\frac{14275935425}{232187904} + \frac{209699405}{2232576} \eta \right) \chi^{-25/9} \right. \\
& + \left(\frac{198510270125}{4493518848} + \frac{1222893635}{12344832} \eta \right) \chi^{-38/9} + \left(\frac{14796093245}{194890752} - \frac{1028884705}{6960384} \eta \right) \chi^{-44/9} \left. \right\} e_0^4 \\
& + \left\{ \left(-\frac{3456734032025}{46950285312} - \frac{216909251525}{1676795904} \eta \right) \chi^{-19/9} + \left(-\frac{2441897241139735}{11858300633088} + \frac{9479155594325}{32577748992} \eta \right) \chi^{-25/9} \right. \\
& + \left(\frac{659649627625375}{2049044594688} + \frac{4063675549105}{5629243392} \eta \right) \chi^{-38/9} + \left(\frac{1968906345873305}{2310624755712} - \frac{8999675405695}{6347870208} \eta \right) \chi^{-44/9}
\end{aligned}$$

$$+ \left(-\frac{3623421822525}{13532659712} - \frac{184463807375}{260243456} \eta \right) \chi^{-19/3} + \left(-\frac{213483902125}{331218944} + \frac{14845156625}{11829248} \eta \right) \chi^{-7} \Big\} e_0^6, \quad (\text{A8c})$$

$$\begin{aligned} \mathcal{E}_{-2} = & -10\pi + \left(\frac{65561\pi}{2880} \chi^{-19/9} - \frac{295945\pi}{19584} \chi^{-28/9} \right) e_0^2 + \left(\frac{217859203\pi}{2626560} \chi^{-19/9} \right. \\ & - \frac{3048212305\pi}{35721216} \chi^{-28/9} - \frac{6211173025\pi}{46227456} \chi^{-38/9} + \frac{1968982405\pi}{13920768} \chi^{-47/9} \Big) e_0^4 + \left(\frac{22156798877\pi}{119771136} \chi^{-19/9} \right. \\ & - \frac{126468066221755\pi}{472377360384} \chi^{-28/9} - \frac{20639727962075\pi}{21079719936} \chi^{-38/9} + \frac{33366234820475\pi}{25391480832} \chi^{-47/9} \\ & \left. + \frac{30628811474315\pi}{32418054144} \chi^{-19/3} - \frac{28409259125\pi}{23658496} \chi^{-22/3} \right) e_0^6. \quad (\text{A8d}) \end{aligned}$$

$$\begin{aligned} \mathcal{E}_{-1} = & \frac{15293365}{1016064} + \frac{27145}{1008} \eta + \frac{3085}{144} \eta^2 + \left\{ \left(-\frac{111064865}{10948608} - \frac{165068815}{3193344} \eta - \frac{10688155}{228096} \eta^2 \right) \chi^{-19/9} + \left(-\frac{5795368945}{227598336} \right. \right. \\ & \left. + \frac{4917245}{1016064} \eta + \frac{25287905}{290304} \eta^2 \right) \chi^{-25/9} + \left(\frac{936702035}{829108224} + \frac{3062285}{145152} \eta - \frac{14251675}{352512} \eta^2 \right) \chi^{-31/9} \Big\} e_0^2 \\ & + \left\{ \left(-\frac{369068546395}{9985130496} - \frac{548523672245}{2912329728} \eta - \frac{35516739065}{208023552} \eta^2 \right) \chi^{-19/9} + \left(-\frac{37202269351825}{192743276544} \right. \right. \\ & - \frac{2132955527705}{48185819136} \eta + \frac{34290527545}{66189312} \eta^2 \Big) \chi^{-25/9} + \left(-\frac{94372278903235}{4047608807424} + \frac{126823556396665}{409579462656} \eta \right. \\ & - \frac{900460970615}{2250436608} \eta^2 \Big) \chi^{-31/9} + \left(\frac{2093389158055165}{82975980552192} + \frac{10817573354545}{30869040384} \eta + \frac{1016830418215}{2713761792} \eta^2 \right) \chi^{-38/9} \\ & + \left(\frac{562379595264125}{2264733499392} + \frac{2965713234395}{40441669632} \eta - \frac{240910046095}{222206976} \eta^2 \right) \chi^{-44/9} + \left(\frac{113287857371225}{1178699268096} \right. \\ & \left. - \frac{4300262795285}{7016067072} \eta + \frac{392328884035}{501147648} \eta^2 \right) \chi^{-50/9} \Big\} e_0^4 \\ & + \left\{ \left(-\frac{187675742904025}{2276609753088} - \frac{278930807554775}{664011177984} \eta - \frac{18060683996675}{47429369856} \eta^2 \right) \chi^{-19/9} \right. \\ & + \left(-\frac{6363444229039638215}{9843784619655168} - \frac{39088433492776445}{175781868208128} \eta + \frac{1550053258427425}{965834440704} \eta^2 \right) \chi^{-25/9} \\ & + \left(-\frac{387035983120116605285}{3263214601415688192} + \frac{1095104635088909345}{747072939884544} \eta - \frac{185468261986684025}{106724705697792} \eta^2 \right) \chi^{-31/9} \\ & + \left(\frac{6956332172217313295}{37837047131799552} + \frac{35946796257153035}{14076282415104} \eta + \frac{3378927479728445}{1237475377152} \eta^2 \right) \chi^{-38/9} \\ & + \left(\frac{74835480932061169625}{26850680368791552} + \frac{14868442349448515}{9220700676096} \eta - \frac{2107245064767505}{202652762112} \eta^2 \right) \chi^{-44/9} \\ & + \left(\frac{43949506831840859555}{24455652414455808} - \frac{1344731894414361455}{145569359609856} \eta + \frac{7946157848161165}{799831646208} \eta^2 \right) \chi^{-50/9} \\ & + \left(-\frac{984783138418096685}{1421880006168576} - \frac{5955948670960595}{2170146521088} \eta - \frac{173415564792655}{51670155264} \eta^2 \right) \chi^{-19/3} \\ & + \left(-\frac{3421718007737775}{1515657887744} - \frac{449229717137975}{284185853952} \eta + \frac{36339370052875}{3122921472} \eta^2 \right) \chi^{-7} \\ & \left. + \left(-\frac{26945014260125}{15650095104} + \frac{17350371000625}{1987313664} \eta - \frac{357715525375}{35487744} \eta^2 \right) \chi^{-23/3} \right\} e_0^6. \quad (\text{A8e}) \end{aligned}$$

Appendix B: Explicit 2PN-accurate expressions for constructing our exact in e_t time-domain approximant

In this appendix, we list explicitly several 2PN-accurate expressions that are required to implement tem-

poral evolutions in $h_+(r, \phi, \dot{r}, \dot{\phi})|_Q$ and $h_\times(r, \phi, \dot{r}, \dot{\phi})|_Q$. We begin by displaying 2PN-accurate parametric expres-

sions for incorporating the radial part of the dynamics:

$$\frac{c^2 r}{G m} = \frac{1 - e_t \cos u}{x} \left\{ 1 + r^{1\text{PN}}(\eta, e_t, u) x + r^{2\text{PN}}(\eta, e_t, u) x^2 \right\}, \quad (\text{B1a})$$

$$\frac{\dot{r}}{c} = \frac{\sqrt{x} e_t \sin u}{1 - e_t \cos u} \left\{ 1 + \dot{r}^{1\text{PN}}(\eta, e_t) x + \dot{r}^{2\text{PN}}(\eta, e_t, u) x^2 \right\}, \quad (\text{B1b})$$

where the PN coefficients are given by

$$r^{1\text{PN}}(\eta, e_t, u) = \frac{-24 + 9\eta + \nu(18 - 7\eta) + e_t^2 [24 - 9\eta + \nu(-6 + 7\eta)]}{6\nu(1 - e_t^2)}, \quad (\text{B2a})$$

$$\begin{aligned} r^{2\text{PN}}(\eta, e_t, u) = & \frac{1}{72\nu(1 - e_t^2)^2} \left\{ -288 + 765\eta - 27\eta^2 + e_t^2(288 - 1026\eta + 54\eta^2) + e_t^4(261\eta - 27\eta^2) \right. \\ & + \left(-540 + e_t^2(540 - 216\eta) + 216\eta \right) \sqrt{1 - e_t^2} + \nu \left[648 - 567\eta + 35\eta^2 \right. \\ & \left. \left. + e_t^2(468 + 150\eta - 70\eta^2) + e_t^4(72 - 231\eta + 35\eta^2) + (180 - 72\eta + e_t^2(-180 + 72\eta)) \sqrt{1 - e_t^2} \right] \right\}, \end{aligned} \quad (\text{B2b})$$

$$\dot{r}^{1\text{PN}}(\eta, e_t) = \frac{-7\eta + e_t^2(-6 + 7\eta)}{6(1 - e_t^2)}, \quad (\text{B2c})$$

$$\begin{aligned} \dot{r}^{2\text{PN}}(\eta, e_t, u) = & \frac{1}{72\nu^3(1 - e_t^2)^2} \left\{ -135\eta + 9\eta^2 + e_t^2(405\eta - 27\eta^2) + e_t^4(-405\eta + 27\eta^2) + e_t^6(135\eta - 9\eta^2) \right. \\ & + \nu \left[-540 + 351\eta - 9\eta^2 + e_t^2(1080 - 702\eta + 18\eta^2) + e_t^4(-540 + 351\eta - 9\eta^2) \right] \\ & + \nu^3 \left[-324 + 189\eta + 35\eta^2 + e_t^2(-234 + 366\eta - 70\eta^2) + e_t^4(72 - 231\eta + 35\eta^2) \right] \\ & \left. - 36\nu^2(3 + \nu)(1 - e_t^2)(-5 + 2\eta) \sqrt{1 - e_t^2} \right\}. \end{aligned} \quad (\text{B2d})$$

In the above expressions ν is a shorthand for $1 - e_t \cos u$.

The angular variables $\dot{\phi}$ and ϕ are given by

$$+ \dot{\phi}^{2\text{PN}}(\eta, e_t, u) x^2 \left. \right\}, \quad (\text{B3a})$$

$$\phi = \lambda + W(\eta, x, e_t, u), \quad (\text{B3b})$$

$$\begin{aligned} W = & (v - u) + e_t \sin u + W^{1\text{PN}}(\eta, e_t, u) x \\ & + W^{2\text{PN}}(\eta, e_t, u) x^2. \end{aligned} \quad (\text{B3c})$$

$$\dot{\phi} = \frac{c^3}{G m} \frac{\sqrt{1 - e_t^2} x^{3/2}}{(1 - e_t \cos u)^2} \left\{ 1 + \dot{\phi}^{1\text{PN}}(\eta, e_t, u) x \right.$$

The 1PN and 2PN parametric contributions to $\dot{\phi}$ and W are given by

$$\dot{\phi}^{1\text{PN}}(\eta, e_t, u) = \frac{(-1 + \nu + e_t^2)(-4 + \eta)}{\nu(1 - e_t^2)}, \quad (\text{B4a})$$

$$\begin{aligned} \dot{\phi}^{2\text{PN}}(\eta, e_t, u) = & \frac{1}{12\nu^3(1 - e_t^2)^2} \left\{ -6(1 - e_t^2)^3(3\eta + 2\eta^2) + \nu \left[108 + 63\eta + 33\eta^2 + e_t^2(-216 - 126\eta - 66\eta^2) \right. \right. \\ & \left. \left. + e_t^4(108 + 63\eta + 33\eta^2) \right] + \nu^2 \left[-240 - 31\eta - 29\eta^2 + e_t^4(-48 + 17\eta - 17\eta^2) + e_t^2(288 + 14\eta + 46\eta^2) \right] \right. \\ & \left. + \nu^3 \left[42 + 22\eta + 8\eta^2 + e_t^2(-147 + 8\eta - 14\eta^2) \right] + 18\nu^2(-2 + \nu + 2e_t^2)(-5 + 2\eta) \sqrt{1 - e_t^2} \right\}, \end{aligned} \quad (\text{B4b})$$

$$W^{1\text{PN}}(\eta, e_t, u) = 3 \frac{e_t \sin u + (v - u)_{1\text{PN}}}{1 - e_t^2}, \quad (\text{B4c})$$

$$W^{2\text{PN}}(\eta, e_t, u) = \frac{e_t \sin u}{32 \nu^3 (1 - e_t^2)^2} \left\{ 4 \nu^2 \left[\nu \left(108 + e_t^2 (102 - 52 \eta) - 56 \eta \right) - 15 \eta + \eta^2 + e_t^2 (30 \eta - 2 \eta^2) \right. \right. \\ \left. \left. + e_t^4 (-15 \eta + \eta^2) \right] + \left[4 \eta - 12 \eta^2 + e_t^2 (-8 \eta + 24 \eta^2) + e_t^4 (4 \eta - 12 \eta^2) \right] \right. \\ \left. + \nu \left(8 + e_t^2 (-8 - 144 \eta) + 144 \eta \right) + \nu^2 \left(-8 - 148 \eta + 12 \eta^2 + e_t^2 (-\eta + 3 \eta^2) \right) \right\} \sqrt{1 - e_t^2}. \quad (\text{B4d})$$

Clearly, we also need to provide the 2PN-accurate parametric expression for $v - u$. As noted in the text, there exists an exact expression for $v - u$ in terms of the ‘angular eccentricity’ e_ϕ [15]:

$$v - u = 2 \tan^{-1} \left[\frac{\beta_\phi \sin u}{1 - \beta_\phi \cos u} \right], \quad (\text{B5})$$

where $\beta_\phi = (1 - \sqrt{1 - e_\phi^2})/e_\phi$. The 2PN-accurate expression for β_ϕ can be written as

$$\beta_\phi = \frac{1 - \sqrt{1 - e_t^2}}{e_t} + \beta_\phi^{1\text{PN}}(\eta, e_t) x + \beta_\phi^{2\text{PN}}(\eta, e_t) x^2, \quad (\text{B6})$$

$$\beta_\phi^{1\text{PN}}(\eta, e_t) = \frac{-4 + \eta + e_t^2 (8 - 2 \eta) + (4 - \eta) \sqrt{1 - e_t^2}}{e_t \sqrt{1 - e_t^2}}, \quad (\text{B7a})$$

$$\beta_\phi^{2\text{PN}}(\eta, e_t) = \frac{1}{96 e_t (1 - e_t^2)^{3/2}} \left\{ -528 - 220 \eta + 4 \eta^2 + e_t^2 (5232 - 1659 \eta + 177 \eta^2) \right. \\ \left. + e_t^4 (-3840 + 2086 \eta - 178 \eta^2) + \left[528 + 220 \eta - 4 \eta^2 + e_t^2 (288 + 83 \eta - 41 \eta^2) \right] \sqrt{1 - e_t^2} \right\}. \quad (\text{B7b})$$

The above listed expressions ensure that the orbital time scale variations in the two GW polarization states are treated in a parametric manner. The temporal evolution of these dynamical variables requires 2PN-accurate Kepler equation and the GW induced variations in x and

where the 1PN and 2PN contributions are given by

e_t .

The PN approximation is also employed to derive the differential equations for x , e_t and l . We display here (again) these three differential equations as

$$\frac{dx}{dt} = \eta \frac{c^3}{Gm} x^5 \left\{ \frac{192 + 584 e_t^2 + 74 e_t^4}{15 (1 - e_t^2)^{7/2}} + \dot{x}^{1\text{PN}}(\eta, e_t) x + \dot{x}^{1.5\text{PN}}(e_t) x^{3/2} + \dot{x}^{2\text{PN}}(\eta, e_t) x^2 \right\}, \quad (\text{B8a})$$

$$\frac{de_t}{dt} = -\eta e_t \frac{c^3}{Gm} x^4 \left\{ \frac{304 + 121 e_t^2}{15 (1 - e_t^2)^{5/2}} + \dot{e}_t^{1\text{PN}}(\eta, e_t) x + \dot{e}_t^{1.5\text{PN}}(e_t) x^{3/2} + \dot{e}_t^{2\text{PN}}(\eta, e_t) x^2 \right\}, \quad (\text{B8b})$$

$$\frac{dl}{dt} = n = x^{3/2} \frac{c^3}{Gm} \left\{ 1 + \dot{l}^{1\text{PN}}(e_t) x + \dot{l}^{2\text{PN}}(\eta, e_t) x^2 \right\}, \quad (\text{B8c})$$

where the PN coefficients are given by

$$\dot{x}^{1\text{PN}}(\eta, e_t) = \frac{-11888 - 14784 \eta + e_t^2 (87720 - 159600 \eta) + e_t^4 (171038 - 141708 \eta) + e_t^6 (11717 - 8288 \eta)}{420 (1 - e_t^2)^{9/2}}, \quad (\text{B9a})$$

$$\begin{aligned} \dot{x}^{2\text{PN}}(\eta, e_t) = & \frac{1}{45360(1-e_t^2)^{11/2}} \left(-360224 + 4514976\eta + 1903104\eta^2 + e_t^2(-92846560 + 15464736\eta + 61282032\eta^2) \right. \\ & + e_t^4(783768 - 207204264\eta + 166506060\eta^2) + e_t^6(83424402 - 123108426\eta + 64828848\eta^2) \\ & \left. + e_t^8(3523113 - 3259980\eta + 1964256\eta^2) - 3024(96 + 4268e_t^2 + 4386e_t^4 + 175e_t^6)(-5 + 2\eta)\sqrt{1-e_t^2} \right), \end{aligned} \quad (\text{B9b})$$

$$\dot{e}_t^{1\text{PN}}(\eta, e_t) = -\frac{67608 + 228704\eta + e_t^2(-718008 + 651252\eta) + e_t^4(-125361 + 93184\eta)}{2520(1-e_t^2)^{7/2}}, \quad (\text{B9c})$$

$$\begin{aligned} \dot{e}_t^{2\text{PN}}(\eta, e_t) = & \frac{1}{30240(1-e_t^2)^{9/2}} \left(-15198032 + 13509360\eta + 4548096\eta^2 + e_t^2(-36993396 - 35583228\eta + 48711348\eta^2) \right. \\ & + e_t^4(46579718 - 78112266\eta + 42810096\eta^2) + e_t^6(3786543 - 4344852\eta + 2758560\eta^2) \\ & \left. - 1008(2672 + 6963e_t^2 + 565e_t^4)(-5 + 2\eta)\sqrt{1-e_t^2} \right), \end{aligned} \quad (\text{B9d})$$

$$j^{1\text{PN}}(e_t) = -\frac{3}{1-e_t^2}, \quad (\text{B9e})$$

$$j^{2\text{PN}}(\eta, e_t) = \frac{-18 + 28\eta + e_t^2(-51 + 26\eta)}{4(1-e_t^2)^2}. \quad (\text{B9f})$$

We note that the 1.5PN order tail contributions, namely $\dot{x}^{1.5\text{PN}}$ and $\dot{e}_t^{1.5}$, are provided by Eq. (3.15).

-
- [1] B. S. Sathyaprakash and B. F. Schutz, *Living Reviews in Relativity* **12**, 2 (2009), 0903.0338.
- [2] The LIGO Scientific Collaboration, J. Aasi, B. P. Abbott, R. Abbott, T. Abbott, M. R. Abernathy, K. Ackley, C. Adams, T. Adams, P. Addesso, et al., *Classical and Quantum Gravity* **32**, 115012 (2015), 1411.4547.
- [3] F. Acernese, M. Agathos, K. Agatsuma, D. Aisa, N. Allemandou, A. Allocca, J. Amarni, P. Astone, G. Balestri, G. Ballardín, et al., *Classical and Quantum Gravity* **32**, 024001 (2015), 1408.3978.
- [4] K. Somiya, *Classical and Quantum Gravity* **29**, 124007 (2012), 1111.7185.
- [5] H.-Y. Chen and D. E. Holz, *Physical Review Letters* **111**, 181101 (2013), 1206.0703.
- [6] P. C. Peters and J. Mathews, *Physical Review* **131**, 435 (1963).
- [7] P. C. Peters, *Phys. Rev.* **136**, B1224 (1964).
- [8] J. H. Taylor, Jr., *Reviews of Modern Physics* **66**, 711 (1994).
- [9] A. Buonanno, B. R. Iyer, E. Ochsner, Y. Pan, and B. S. Sathyaprakash, *Phys. Rev. D* **80**, 084043 (2009), 0907.0700.
- [10] E. A. Huerta, P. Kumar, S. T. McWilliams, R. O’Shaughnessy, and N. Yunes, *Phys. Rev. D* **90**, 084016 (2014), 1408.3406.
- [11] J. Samsing, M. MacLeod, and E. Ramirez-Ruiz, *Astrophys. J.* **784**, 71 (2014), 1308.2964.
- [12] R. M. O’Leary, B. Kocsis, and A. Loeb, *Monthly Notices of the Royal Astronomical Society* **395**, 2127 (2009), 0807.2638.
- [13] W. H. Lee, E. Ramirez-Ruiz, and G. van de Ven, *Astrophys. J.* **720**, 953 (2010), 0909.2884.
- [14] N. Yunes, K. G. Arun, E. Berti, and C. M. Will, *Phys. Rev. D* **80**, 084001 (2009), 0906.0313.
- [15] C. Königsdörffer and A. Gopakumar, *Phys. Rev. D* **73**, 124012 (2006), gr-qc/0603056.
- [16] M. Boyle, D. A. Brown, L. E. Kidder, A. H. Mroué, H. P. Pfeiffer, M. A. Scheel, G. B. Cook, and S. A. Teukolsky, *Phys. Rev. D* **76**, 124038 (2007), 0710.0158.
- [17] T. Damour, B. R. Iyer, and B. S. Sathyaprakash, *Phys. Rev. D* **57**, 885 (1998), gr-qc/9708034.
- [18] L. Blanchet, *Living Reviews in Relativity* **17**, 2 (2014), 1310.1528.
- [19] L. Blanchet, T. Damour, and B. R. Iyer, *Phys. Rev. D* **51**, 5360 (1995), gr-qc/9501029.
- [20] L. Blanchet, T. Damour, G. Esposito-Farèse, and B. R. Iyer, *Physical Review Letters* **93**, 091101 (2004), gr-qc/0406012.
- [21] L. Blanchet, G. Faye, B. R. Iyer, and S. Sinha, *Classical and Quantum Gravity* **25**, 165003 (2008), 0802.1249.
- [22] E. A. Huerta and D. A. Brown, *Phys. Rev. D* **87**, 127501 (2013), 1301.1895.
- [23] C. M. Bender and S. A. Orszag, *Advanced Mathematical Methods for Scientists and Engineers* (1978).
- [24] A. Królak, K. D. Kokkotas, and G. Schäfer, *Phys. Rev. D* **52**, 2089 (1995), gr-qc/9503013.
- [25] T. Damour and N. Deruelle, *Ann. Inst. Henri Poincaré Phys. Théor.*, Vol. 43, No. 1, p. 107 - 132 **43**, 107 (1985).
- [26] R.-M. Memmesheimer, A. Gopakumar, and G. Schäfer, *Phys. Rev. D* **70**, 104011 (2004), gr-qc/0407049.
- [27] T. Damour, A. Gopakumar, and B. R. Iyer, *Phys. Rev. D* **70**, 064028 (2004), gr-qc/0404128.
- [28] I. Hinder, F. Herrmann, P. Laguna, and D. Shoemaker, *Phys. Rev. D* **82**, 024033 (2010), 0806.1037.
- [29] S. Mikkola, *Celestial Mechanics* **40**, 329 (1987).

- [30] L. Blanchet and G. Schafer, *Classical and Quantum Gravity* **10**, 2699 (1993).
- [31] R. Rieth and G. Schäfer, *Classical and Quantum Gravity* **14**, 2357 (1997).
- [32] M. Tessmer and A. Gopakumar, *Phys. Rev. D* **78**, 084029 (2008), 0712.3199.
- [33] H. Wahlquist, *General Relativity and Gravitation* **19**, 1101 (1987).
- [34] K. S. Thorne, *Gravitational radiation* (1989), p. 330.
- [35] W. Junker and G. Schaefer, *Monthly Notices of the Royal Astronomical Society* **254**, 146 (1992).
- [36] K. G. Arun, L. Blanchet, B. R. Iyer, and S. Sinha, *Phys. Rev. D* **80**, 124018 (2009), 0908.3854.
- [37] M. Favata, *Physical Review Letters* **112**, 101101 (2014), 1310.8288.
- [38] A. Gopakumar and B. R. Iyer, *Phys. Rev. D* **65**, 084011 (2002), gr-qc/0110100.
- [39] M. Tessmer and A. Gopakumar, *Monthly Notices of the Royal Astronomical Society* **374**, 721 (2007), gr-qc/0610139.
- [40] T. Damour and G. Schafer, *Nuovo Cimento B Serie* **101**, 127 (1988).
- [41] K. G. Arun, L. Blanchet, B. R. Iyer, and M. S. S. Quisailah, *Phys. Rev. D* **77**, 064035 (2008), 0711.0302.
- [42] A. Gopakumar and B. R. Iyer, *Phys. Rev. D* **56**, 7708 (1997), gr-qc/9710075.
- [43] D. Bini and T. Damour, *Phys. Rev. D* **86**, 124012 (2012), 1210.2834.
- [44] B. J. Owen, *Phys. Rev. D* **53**, 6749 (1996), gr-qc/9511032.
- [45] G. M. Harry and LIGO Scientific Collaboration, *Classical and Quantum Gravity* **27**, 084006 (2010).
- [46] B. Moore, M. Favata, K. Arun, and C. Mishra (2015), in preparation.
- [47] M. Tessmer and G. Schäfer, *Phys. Rev. D* **82**, 124064 (2010), 1006.3714.
- [48] M. Tessmer and G. Schäfer, *Annalen der Physik* **523**, 813 (2011), 1012.3894.
- [49] A. Gopakumar and G. Schäfer, *Phys. Rev. D* **84**, 124007 (2011).
- [50] P. Cszimadia, G. Debreczeni, I. Rácz, and M. Vasúth, *Classical and Quantum Gravity* **29**, 245002 (2012), 1207.0001.
- [51] B. Kocsis and J. Levin, *Phys. Rev. D* **85**, 123005 (2012), 1109.4170.
- [52] W. E. East, S. T. McWilliams, J. Levin, and F. Pretorius, *Phys. Rev. D* **87**, 043004 (2013), 1212.0837.
- [53] S. Klimentenko, I. Yakushin, A. Mercer, and G. Mitselmakher, *Classical and Quantum Gravity* **25**, 114029 (2008), 0802.3232.
- [54] K. S. Tai, S. T. McWilliams, and F. Pretorius, *Phys. Rev. D* **90**, 103001 (2014), 1403.7754.
- [55] M. Coughlin, P. Meyers, E. Thrane, J. Luo, and N. Christensen, *Phys. Rev. D* **91**, 063004 (2015), 1412.4665.